


Full length article

Enhancing Human-Robot Collaborative Transportation of Deformable Objects using Multi-modal Reinforcement Learning and Adaptive Admittance Control

Qi Zhou, Bohan Feng, Boyan Li, Chang Liu, Yulin Chen, Youyi Bi ^{*} 

Global College, Shanghai Jiao Tong University, Shanghai 200240, China

ARTICLE INFO

Keywords:

Human-robot collaboration
Deformable object handling
Multi-Modal state representation
Reinforcement learning
Robot motion planning
Admittance control

ABSTRACT

Human-robot collaborative transportation (HRCT) of deformable objects is critical for improving production efficiency, reducing human workload, and enhancing operational safety in the context of handling delicate or flexible materials. However, traditional passive compliance control methods often suffer from decreased control accuracy and inadequate tracking performance in complex tasks, while proactive motion control approaches are sensitive to environment interference and lack stability. To address these issues, we propose a novel HRCT approach for deformable objects based on multi-modal reinforcement learning (RL) and adaptive admittance control, termed as Collaborative Deformable-Object Transportation (CoDoT). This approach combines proactive motion planning with adaptive compliance control, improving the compliance and stability in human-robot collaborative transportation tasks, effectively reducing object deformation and ensuring safe human-robot interaction. Specifically, the proactive motion planning module integrates multi-modal (including force/torque and tactile feedback) state representation with RL-based motion control. In addition, an adaptive admittance controller dynamically adjusts the admittance parameters based on the object's deformation and robot's motion fluctuations to balance the compliance and stability of transportation. The proposed approach is examined and evaluated in both simulated and real-world scenarios. The experimental findings indicate that our approach effectively enhances HRCT of deformable objects in operational accuracy, stability, and deformation control capability compared to traditional RL-based control models and admittance control methods.

1. Introduction

The human-centered philosophy empowering the collaboration between humans and machines, has become the cornerstone of next-generation manufacturing mode such as Industry 5.0 [1]. In this context, Human-Robot Collaborative Transportation (HRCT), as a key technology for efficient and safe material handling, is increasingly being applied across various manufacturing sectors, such as electronics and aerospace manufacturing industry [2]. Although pure robotic transportation may excel in efficiency, it faces challenges in handling soft and deformable objects that require precise control. Meanwhile, manual transportation, though more adaptable, often requires more labor force for efficient handling in high-intensity tasks and could pose risks to

human workers' health. By combining the strengths of robots and humans, HRCT overcomes these limitations, leading to enhanced production efficiency, reduced human workload, improved human-robot interaction safety, and decreased human operational errors.¹

HRCT tasks can be categorized into three types based on the rigidity of the handled objects: rigid objects (e.g., wooden sticks, metal parts), highly deformable objects (e.g., ropes, fabrics, which can withstand stretching but not compression), and partially deformable objects (e.g., silicone rods, composite materials) [3]. There have been extensive research on HRCT for rigid and highly deformable objects [4,5]. However, studies involving partially deformable objects remain relatively limited. HRCT for partially deformable objects holds significant potential for applications in many industrial areas, such as precision

^{*} Corresponding author.

E-mail addresses: zhouqi1998@sjtu.edu.cn (Q. Zhou), bohan.feng@sjtu.edu.cn (B. Feng), liboyan@sjtu.edu.cn (B. Li), fzcowen1@sjtu.edu.cn (C. Liu), chenyulin@sjtu.edu.cn (Y. Chen), youyi.bi@sjtu.edu.cn (Y. Bi).

¹ See real-world examples of Human-Robot Collaborative Transportation: <https://www.youtube.com/watch?v=LRiNIUZUAa0>, https://www.youtube.com/watch?v=tLQ_AulO0Ag.

<https://doi.org/10.1016/j.aei.2025.103905>

Received 24 January 2025; Received in revised form 14 May 2025; Accepted 16 September 2025

Available online 24 September 2025

1474-0346/© 2025 Elsevier Ltd. All rights are reserved, including those for text and data mining, AI training, and similar technologies.

engineering (e.g., transportation of flexible films) and electronics manufacturing (e.g. handling of soft sensors and integrated circuit boards). Compared to rigid objects, partially deformable objects exhibit more intricate deformation characteristics in handling tasks. Precise control strategies are required to prevent irreversible deformations or damage of these objects, while highly deformable objects such as fabrics usually can tolerate much larger deformation. Therefore, the robot control for handling partially deformable objects is more complex.

Existing methods of HRCT for partially deformable objects primarily rely on force or position feedback for passive compliance control [6] or proactive motion planning [7]. While passive compliance methods perform well in simple tasks, they often suffer from decreased control accuracy and inadequate tracking performance in more complex tasks, particularly in handling partially deformable objects. This is mainly due to the inability of Force/Torque (F/T) sensors (usually installed on the wrist of a robot arm) to detect local contact information and the attenuation of force/torque signals being transmitted from the deformation end to the fixed end (imagine a rubber rod gasping by a robotic arm). On the other hand, proactive motion planning methods, which can predict human intent to enable flexible control, often suffer from insufficient stability. These methods are highly susceptible to environmental changes (e.g., uncertainty in human motion speed and force due to unstable grasping during transportation), which can significantly affect their performance. Therefore, balancing compliance and stability in handling partially deformable objects remains a critical challenge.

In deformable-object manipulation, accurately and comprehensively representing the state of the object is a fundamental need. Current methods predominantly rely on vision systems to capture shape changes [8]. However, ordinary industrial cameras often struggle with detecting small-scale deformations and handling interference and occlusion issues, which restricts their practical applicability. Consequently, adopting non-vision sensing for deformable-object's state representation is of great practical significance. Such methods could overcome the limitations of visual perception and provide more reliable information for the precise manipulation of deformable objects.

To address these challenges, we propose a novel HRCT approach for partially deformable objects based on multi-modal reinforcement learning (RL) and adaptive admittance control, termed as Collaborative Deformable-Object Transportation (CoDoT). This approach combines proactive motion planning and adaptive compliance control, enhancing both the compliance and stability of human-robot collaborative transportation tasks while effectively reducing object deformation during transportation and improving human-robot collaboration safety. Specifically, we develop a proactive motion planning model based on multi-modal state representation and RL. Instead of using visual sensing, this method employs force/torque and tactile information jointly to accurately represent the state of the soft object and generate robot control strategies. Additionally, the model is enhanced with a domain adapter to improve its adaptability to handling objects with varying stiffnesses. We also propose an adaptive admittance controller that dynamically adjusts the admittance parameters to balance compliance and stability. Experimental results demonstrate that our approach significantly outperforms traditional RL-based control methods and admittance control methods in terms of operational accuracy, stability, and object deformation control. The main contributions of this work include:

- A novel human-robot collaborative transportation approach for partially deformable objects is proposed. This approach combines proactive motion planning and adaptive compliance control, which can significantly reduce the collaborative burden on operators and improve operational comfort and safety.
- A proactive robot motion planning model based on multi-modal state representation and reinforcement learning is developed. This model enhances real-time perception of soft object's states and improves the robot's active compliance and adaptability.

- An adaptive admittance controller is designed. This controller introduces deformation and stability factors to dynamically adjust admittance parameters, thereby balancing compliance and stability in human-robot collaboration.

The rest of this paper is organized as follows. Section 2 reviews related work in human-robot collaborative transportation, methods for soft object manipulation and admittance control. Section 3 introduces the architecture of the proposed approach and explains its key components. Section 4 presents the simulation and real-world experimental setups to validate our approach, and provides a detailed discussion of the experimental results. Section 5 summarizes our work and highlights potential future research directions.

2. Related work

2.1. Human-robot collaborative transportation

Passive compliance control is one of the most commonly used control strategies in Human-Robot Collaborative Transportation (HRCT) tasks. It relies on force/torque (F/T) sensors to measure external forces and achieves compliance control through F/T feedback or elastic mechanical components (e.g., spring, damper) [9–11]. For example, Hirata et al. [12] developed a passive robot porter, where servo brakes respond to the external forces exerted by operator, enabling compliant manipulation of objects to follow human motion. Similarly, Nemec et al. [13] adjusted the robot's stiffness in the operational workspace, allowing the robot to exhibit passive compliance during collaborative tasks. Ikeura and Inooka [14] utilized variable impedance control for human-robot collaboration, where impedance parameters are adaptively switched to meet the requirements of different task stages. While these passive compliance control methods can offer adaptability and safety for uncomplicated HRCT tasks, their performance heavily depend on the external forces applied, lacking proactive environmental perception and predictive capabilities. As a result, they perform poorly in complex and dynamic environments [3].

In contrast, proactive control methods enhance autonomy and intelligence by actively sensing environmental changes and predicting human intentions to coordinate the robot's movements. These methods typically employ cameras [15] and tactile sensors [16] to perceive environmental states. Some researches utilize wearable sensors to monitor human muscle activity [17] and posture changes [18], thereby predicting human behavior and adjusting control strategies accordingly. However, proactive control methods often face challenges in stability, especially when confronted with sudden environmental changes or highly noisy sensor data. In such cases, these methods may lead to dangerous robot actions, potentially causing damage to the manipulated objects and compromising the safety of human-robot collaboration.

Recently, hybrid control methods that combine passive compliance with proactive control have significantly improved the adaptability and stability of human-robot collaboration systems. For example, Kim et al. [19] designed a novel safety joint module that actively responds to collisions and passively absorbs shock forces through mechanical components. However, the collision detection threshold needs to be manually set in their work, which may not adapt well to dynamic scenarios. Sirintuna et al. [3] presented an object deformation-agnostic HRCT framework, where human intentions are inferred based on tactile and motion capture data, and collaboration for handling objects with varying stiffness is achieved via admittance control. However, this method requires humans to wear motion capture devices, which can limit the flexibility and efficiency of human operators. Additionally, Bussy et al. [20] proposed a method in which robots can switch between "leader" and "follower" roles, but the flexibility of robot movement is constrained by pre-defined rules. To address these issues, we expect to develop a hybrid control strategy that integrates proactive robot motion planning and adaptive admittance control. This strategy aims to enhance the

robot's adaptability to dynamic environments while improving the collaboration compliance and system stability.

2.2. Soft object manipulation

In human-robot collaborative manipulation tasks involving soft objects, the nonlinear dynamics and deformable characteristics of these objects impose higher demands on robotic perception and control. Soft object state estimation methods can be categorized into model-based and learning-based methods. Model-based methods predict the deformation of soft objects by constructing dynamics models. For example, Aksoy and Wen [21] employed a position-based dynamics model to predict the motion of soft materials. Andronas et al. [22] simulated fabric deformation using a mass-spring model to enable collaborative manipulation of fabrics. Additionally, Sirintuna et al. [23] integrated tactile feedback and human kinematic information to create an adaptive control framework that can respond in real time to unknown deformations of soft targets. Besides, Finite Element Analysis (FEA) has been widely used for simulating soft object deformations, providing a theoretically precise description of the deformation process [24,25]. However, physical modeling approaches often rely on complex prior knowledge, entail significant computational costs, and lack real-time performance [26], which limits their practical applicability in dynamic scenarios.

Recently, data-driven methods have become increasingly popular for learning deformation patterns of soft objects from large-scale datasets. For instance, Zhou et al. [27] proposed a method based on topological latent representations and sliding mode control to achieve shape control of deformable objects. Nicola et al. [8] employed convolutional neural networks (CNNs) to process depth images for real-time cloth deformation estimation. Furthermore, reinforcement learning (RL), with strong self-learning capability through interaction with the environment, has also demonstrated advantages in soft object manipulation. For example, Laezza and Karayiannidis [28] utilized the Deep Deterministic Policy Gradient (DDPG) algorithm to solve the problem of elastoplastic soft object manipulation by incorporating intrinsic shape features. Scheikl et al. [29] applied pixel-level domain adaptation for simulating-to-real visual transfer, advancing human-robot collaboration in medical surgery. However, these methods often rely on visual information, which in practical applications are prone to limitations due to occlusion and image detection accuracy, and struggle to precisely capture state changes of soft objects in dynamic environments.

To address the limitations of vision-based detection methods, researchers have explored using force or tactile sensors for state estimation and control of soft objects. For example, Sanchez et al. [30] utilized tactile sensors to track soft object deformations in real time and update the deformation model based on contact forces. Süßerkrüb et al. [31] combined tactile sensing with dynamic models to enable online shape updating. However, most of these methods rely on single sensor types, limiting their ability to comprehensively capture the complex states of soft objects, especially in dynamic environments with large deformations or noisy sensor data. To overcome these limitations, we expect to develop a novel proactive motion planning method based on multi-modal perception and reinforcement learning. This method integrates force and tactile information to accurately represent the state of soft targets and utilizes RL to achieve proactive human-robot collaborative transportation in dynamic environments.

2.3. Compliance control methods in human-robot collaboration

Compliance control strategies, such as admittance control and impedance control, have been widely adopted in human-robot collaboration tasks due to their ability to ensure safe and efficient interaction between human and robots. Admittance control regulates the robot's displacement or velocity based on external force/torque sensor feedback, making it particularly suitable for tasks that require precise force

tracking. In contrast, impedance control modulates the interaction dynamics through the stiffness, damping, and inertia characteristics of the mechanical system, making it more effective for motion tracking tasks, such as tool handling or trajectory following, where precise position control is essential [32]. In the context of HRCT, admittance control is more applicable, as it allows for real-time adjustment of robot motion in response to varying forces exerted by the human, thus ensuring the operational comfort and safety of human workers.

However, these methods typically rely on fixed parameters, such as stiffness and damping [33,34], which limits their adaptability to dynamic environments or variations in human motion, thereby reducing the smoothness of human-robot collaboration. To enhance the adaptability of compliance control, parameter-varying compliance control strategies have been proposed. For instance, Park et al. [34] introduced an impedance control framework that estimates and adjusts object impedance in real-time based on online estimation of object's physical parameters (e.g., mass, center of mass, moment of inertia), thereby improving collaboration performance in complex tasks. Furthermore, Huang et al. [35] proposed an adaptive impedance control method that dynamically adjusted the stiffness coefficient based on the robot's end-effector position to ensure control stability and compliance. Other methods combine reinforcement learning with model predictive control to optimize impedance parameters, significantly improving interaction performance [36,37]. Additionally, some approaches integrate visual and force sensor information to implement nonlinear control for smooth end-effector tracking [38]. However, these methods are primarily designed for rigid objects and exhibit limitations when applied to deformable objects.

In recent years, variable admittance control has gradually been applied to human-robot collaboration tasks involving deformable objects. For example, Sirintuna et al. [23] combined admittance control with hand velocity to dynamically generate reference velocities that adapt to objects with different deformation characteristics, but this approach neglects deformation information, which could potentially damage the manipulated object. Tang et al. [39] utilized a gray prediction model to adjust the reference position in real-time, reducing steady-state force errors to improve soft object grasping accuracy. However, this method struggles to adapt to dynamic environments especially when the manipulated object's position changes rapidly. To address these limitations, we expect to propose an adaptive admittance controller that introduces deformation and stability factors, enabling dynamic adjustment of admittance parameters and significantly improving both compliance and stability in human-robot collaboration.

3. Methods

3.1. Overall structure of the proposed approach

Fig. 1 presents the overall structure of the proposed Collaborative Deformable-Object Transportation Approach (CoDoT), which consists of three main modules: Perception, Proactive Motion Planning and Compliance Control. The Proactive Motion Planning module includes domain adapter, multi-modal encoder, deformation predictor, and reinforcement learning (RL) model. This module utilizes multi-modal sensing inputs provided by the Perception module to make intelligent decisions regarding the motion planning of the robot. The Compliance Control module employs an adaptive admittance controller that can dynamically adjust the admittance control parameters, enabling compliant control with enhanced adaptability. The Proactive Motion Planning Module and the Compliance Control Module work synergistically in human-robot collaborative transportation tasks. The former provides adaptive and proactive following capability through motion strategies generated from the RL model, while the latter ensures system responsiveness and stability through adaptive admittance controller. For simplicity, the terms "soft" and "deformable" are used to refer to "partially deformable" in the following sections.

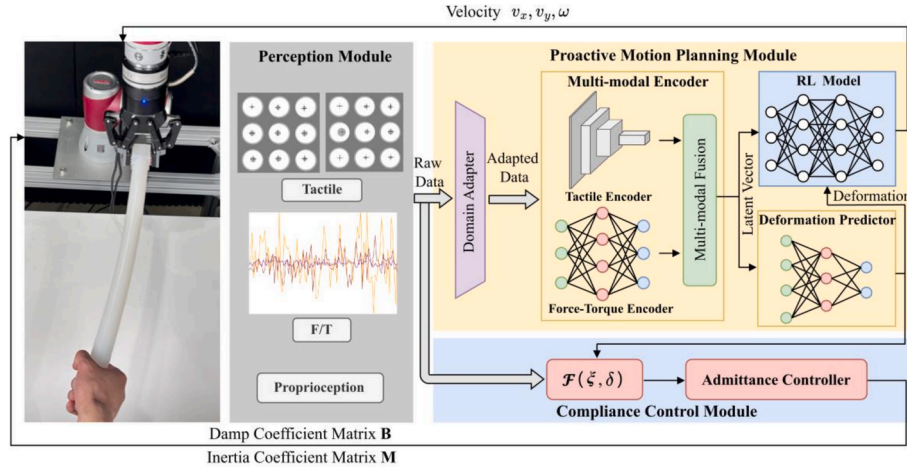


Fig. 1. Overall structure of the proposed Collaborative Deformable-Object Transportation Approach (CoDoT).

In this approach, a silicone rod is selected as a representative soft object for transportation due to its well-defined physical properties (e.g., shape and elasticity). Additionally, the silicone rod offers a controlled and repeatable test scenario, making it ideal for evaluating the performance of our approach. By utilizing the domain adapter (as described in Section 3.4), our approach is capable of handling a wide variety of soft objects. This adaptability ensures that our method can be smoothly applied to other similar deformable objects (e.g., flexible bars and soft boards), making it highly versatile and suitable for diverse industrial applications.

The whole system works as follows: initially, the tactile data and force/torque (F/T) data are input to the domain adapter, which maps them to a standardized reference object data distribution. The adapted data is then passed to the multi-modal encoder and deformation predictor to extract target object features and predict the deformation of the soft object. This information is further input into the RL model to support robot motion planning. Simultaneously, the admittance controller

dynamically adjusts the admittance control parameters based on the F/T data, motion states of robot (e.g., displacement, velocity, and acceleration), and the deformation information, thereby ensuring stable compliant control. The key techniques involved in this approach are described in detail in the following subsections.

3.2. State representation and deformation prediction model for soft object

Obtaining the accurate status of the object is crucial for efficient control in soft-object manipulation tasks. As a key indicator of the target object's physical state, deformation is essential for assessing the stability and adaptability of human-robot collaborative transportation (HRCT) of soft objects. We propose a multi-modal state representation and deformation prediction model to capture surface contact information and deformation characteristics of target object, supporting efficient training of the RL-based motion planning model and precise control by the admittance controller. The architecture of this module is illustrated in

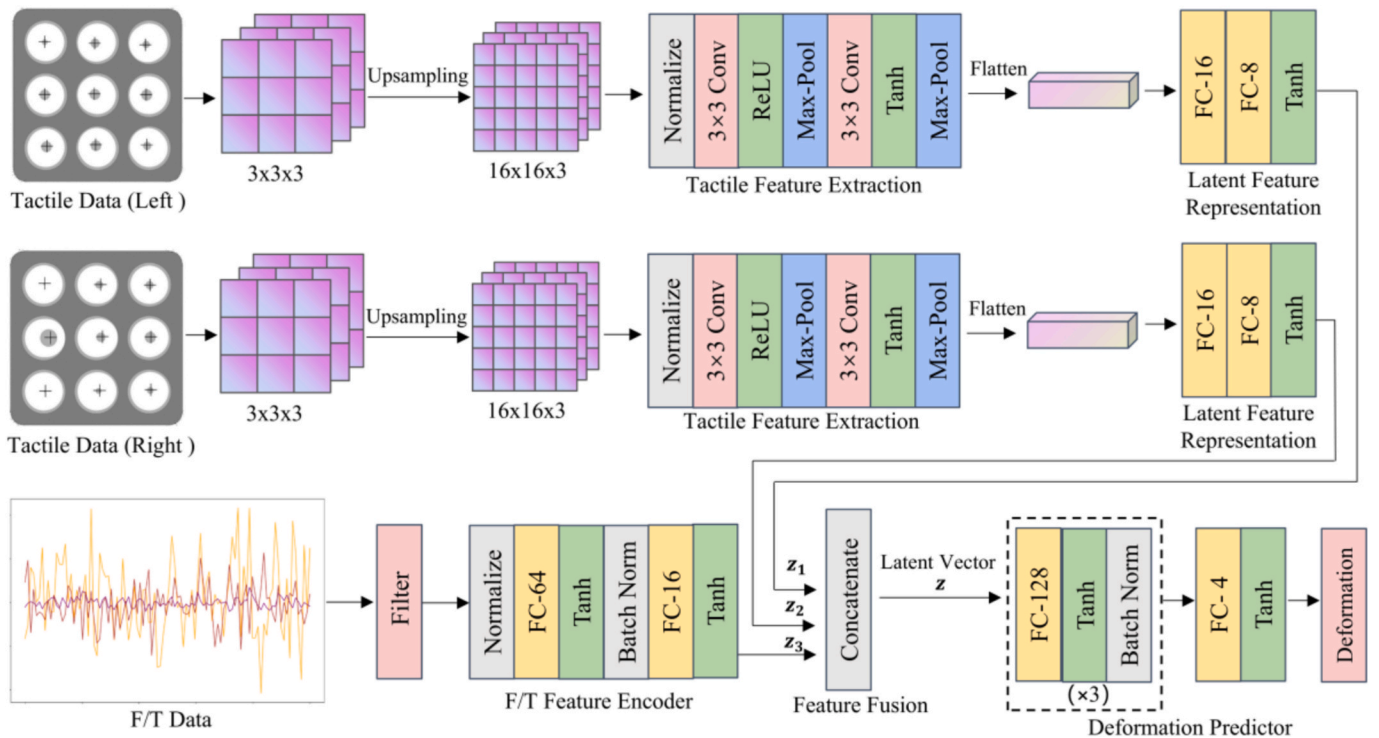


Fig. 2. The architecture of the multi-modal state representation and deformation prediction model.

Fig. 2.

Specifically, the module encodes two types of sensor data: tactile data from the robot gripper, and force/torque (F/T) data from the robot's wrist joint. Given the distinct characteristics of each modality, dedicated encoders are designed for extracting features from each type of data. For tactile feedback, a Convolutional Neural Network (CNN) is employed to extract features from the tactile data and capture the relationship between the spatial distribution of tactile signals and the state of soft object. First, tactile data from both sides are integrated into $3 \times 3 \times 3$ tensors, where each layer of the tensor represents force measurements along the x , y and z axes. Considering the scenario where the contact area of soft object and the tactile sensor is flat, the force distribution on the tactile sensor's surface is expected to exhibit smooth and continuous characteristics [40]. Bilinear interpolation is applied to upsample the tactile data, enhancing its resolution and continuity, thereby improving the fine-grained feature extraction. The upsampled tactile data is then passed through a convolutional module for feature extraction, where the input data is first normalized. Two 3×3 convolutional layers, ReLU and Tanh activation functions, and a max-pooling layer are sequentially applied to extract tactile features. The resulting feature vectors are then passed through a two-layer fully connected network, which performs dimensionality reduction and outputs the final feature vectors \mathbf{z}_1 and \mathbf{z}_2 . It is important to note that, to avoid confusion between the left and right tactile data during concatenation, we independently encode the left and right sides. For F/T feedback, the forces (F_x, F_y, F_z) and torques (T_x, T_y, T_z) are first smoothed using a Low-pass filter and then passed through a two-layer Multi-layer Perceptron (MLP) to obtain the feature vector \mathbf{z}_3 .

In the fusion module, the tactile feature vectors \mathbf{z}_1 and \mathbf{z}_2 , along with the F/T feature vector \mathbf{z}_3 , are concatenated along the feature dimension to form a unified latent representation vector \mathbf{z} , which is then input to the deformation predictor to forecast the target object's deformation. The deformation predictor consists of a three-layer MLP network. We employ a supervised learning framework to jointly train the encoder and predictor to minimize the deformation prediction error.

3.3. Reinforcement learning model for proactive motion planning

To enhance the proactive collaboration performance of the robot, a

motion planning module based on Reinforcement Learning (RL) is developed. In this module, the robot is treated as an intelligent agent that learns to take actions through interaction with environment. Leveraging RL's strong self-learning capabilities, our approach improves the adaptability and efficiency of robotic systems in dynamic transportation environments.

The training process for the proactive motion planning module is depicted in Fig. 3. The RL model is trained within the Unity platform, which provides a flexible virtual environment for robot motion training. A linear rail-slider system is also incorporated to simulate human hand's motion, with the robot arm and slider each holding one end of the object. To overcome the limitations of conventional robotic simulation platforms (e.g., lack of high-precision simulations of force and tactile feedback), we introduce a pre-trained Force-Tactile Predictor to predict both tactile and force/torque (F/T) signals. The Force-Tactile Predictor is implemented as an MLP network with four fully connected layers, where each layer comprises 128 neurons. It receives the position data of the robot's end effector (gripper) and the slider as inputs, and outputs the corresponding tactile data as well as F/T measurements. This pre-trained model enables the simulation of realistic tactile and force signals, facilitating more accurate and reliable training for the RL-based motion planning module.

The RL training process is as follows, the rail-slider system generates random translational motion along the x and y axes, as well as rotational motion around the z -axis, which is provided by a rotatable platform on the rail's slider. The robot's and slider's position, $\mathbf{P}_{robot} = (x_{robot}, y_{robot}, \theta_{robot})$, $\mathbf{P}_{slider} = (x_{slider}, y_{slider}, \theta_{slider})$ are input to Force-Tactile predictor to predict the force/torque signal $\mathbf{F} = (F_x, F_y, F_z)$, $\mathbf{T} = (T_x, T_y, T_z)$ and tactile signal \mathbf{H} . These data are then fed into the pre-trained Multi-modal Encoder and Deformation Predictor network to generate the latent vector \mathbf{z} and the deformation δ of the soft object, respectively. The latent vector \mathbf{z} serves as the RL state, while the deformation δ is used to compute the reward function. The RL model outputs robot action \mathbf{a} , which is then used in conjunction with inverse kinematics to solve for the joint angles and update the robot's pose. The parameters of the Force-Tactile predictor, Multi-modal Encoder, and Deformation Predictor models remain frozen during RL training, which is a common strategy in robot control area to reduce training costs [41].

We employ Proximal Policy Optimization (PPO) [42] as the RL

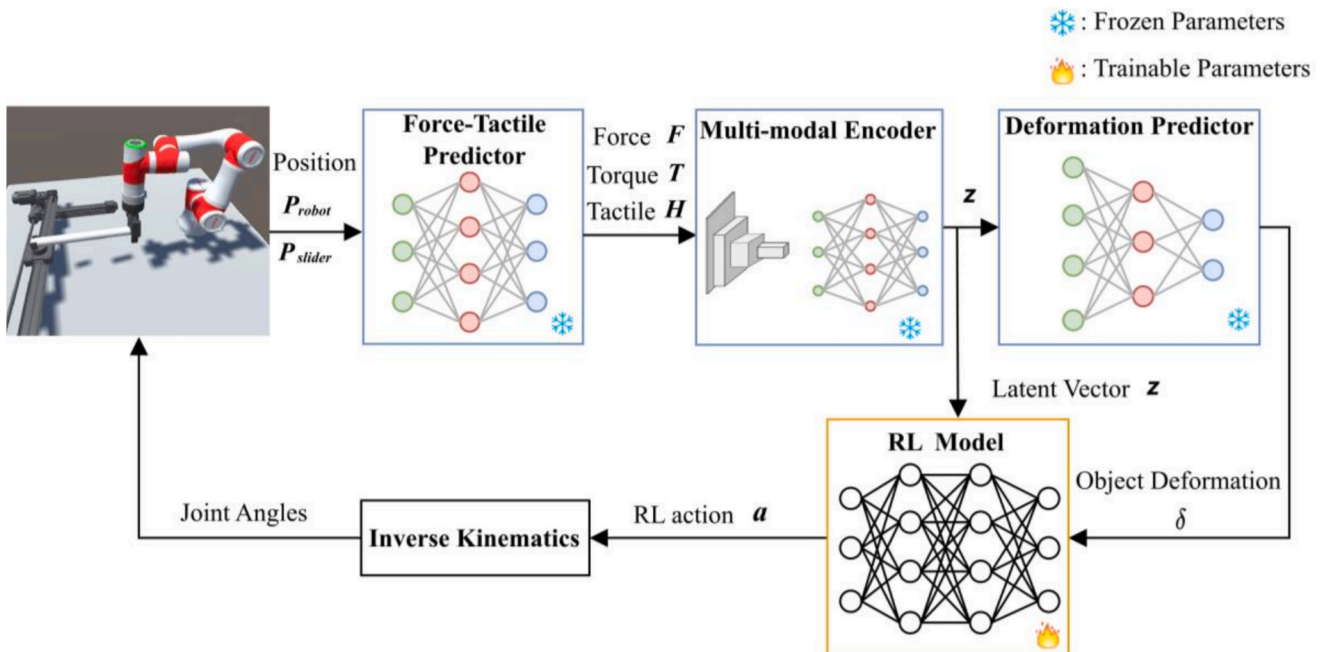


Fig. 3. Training process of proactive robot motion planning module.

algorithm due to its superior efficiency and stability in handling complex decision-making tasks. PPO improves training stability by clipping the probability ratio during policy updates, thus limiting the magnitude of updates. This helps to enhance training efficiency while preventing abrupt changes in model performance. Additionally, PPO incorporates an advantage function estimate, which effectively reduces the variance in policy updates, making it particularly well-suited for decision-making in dynamic and complex environments. The definitions of the state, action, and reward function of the RL model are as follows:

State:

$$\mathbf{s} = \mathbf{z} = [z_1, z_2, \dots, z_{32}] \quad (1)$$

Action:

$$\mathbf{a} = [v_x, v_y, \omega] \quad (2)$$

where,

v_x : Robot velocity along x axis.

v_y : Robot velocity along y axis.

ω : Robot angular velocity along z axis.

Reward function:

$$r = -\lambda_1 \sum_{i=1}^n |\delta_i| + \lambda_2 C + P_1 + P_2 \quad (3)$$

where,

$$P_1 = \begin{cases} 10 & \text{if } C = C_{max} \\ 0 & \text{if } C < C_{max} \end{cases} \quad (4)$$

$$P_2 = \begin{cases} -10 & \text{if } D_x > \sigma_x \text{ or } D_y > \sigma_y \text{ or } D_\theta > \sigma_\theta \\ 0 & \text{else} \end{cases} \quad (5)$$

$$D_x = |x_{slider} - x_{robot}| \quad (6)$$

$$D_y = |y_{slider} - y_{robot}| \quad (7)$$

$$D_\theta = |\theta_{slider} - \theta_{robot}| \quad (8)$$

δ_i represents the deformation magnitude of the soft object along different directions, λ_1 and λ_2 are positive weighting coefficients. C denotes the current step number in training episode, while C_{max} refers to the episode length. P_1 is the task completion reward function, and P_2 is a penalty function used to penalize cases where the relative position between the robot and the slider exceeds the specified range. D_x , D_y , D_θ , σ_x , σ_y , σ_θ represent the relative distances along the x and y axes and the angular deviation along the z axis between the slider and the robot's end-effector, along with the corresponding boundary thresholds. As the target's deformation decreases, the reward increases. $\lambda_2 C$ is introduced to incentivize the robot to consistently follow the slider. Upon episode completion, if the robot remains within the specified distance from the slider, a task completion reward is applied. Furthermore, if the relative distance or angular deviation between the robot and slider exceeds the defined threshold, a penalty is triggered, enforcing strict constraints on the robot's following deviation.

3.4. Domain adapter

As mentioned earlier, deformation information is critical to the subsequent motion planning and compliance control in our system. However, identical force will result in different deformations of soft objects with various stiffness and shapes, and our system only uses the force/torque and tactile data of a reference soft object to train all state representation, deformation prediction and motion planning models. Directly utilizing the force/torque and tactile data of a new soft object as the input will lead to errors in computing the encoded latent state vector and predicting the deformation. To solve this issue, we propose a

domain adapter to compensate the influence of a new object's stiffness and shape on its deformation. This approach enables efficient reuse of pre-trained neural network models, enhancing the adaptability and generalization of the robot's proactive motion planning across different soft objects.

Soft materials typically exhibit elastic behavior within small deformation ranges. The robot-object-human system in collaborative transportation can be approximated as a cantilever beam model, as shown in Fig. 4. In this model, a cantilever beam of length L is fixed at one end by the robot gripper, while a load F is applied perpendicular to the beam's free end by human, causing a displacement u at the beam's tip.

For the reference elastic rod, assuming it is subjected to a vertical load F_r , and based on beam bending theory, the displacement at the tip u_r can be approximated as:

$$u_r = \frac{F_r L_r^3}{3E_r I_r} = \frac{F_r}{k_r} \quad (9)$$

where L_r , E_r , I_r represent the length, Young's modulus, and area moment of inertia of the reference elastic rod, respectively, and k_r is the equivalent flexural stiffness.

Similarly, for a different elastic rod, the displacement at the tip can be approximated as:

$$u_i = \frac{F_i L_i^3}{3E_i I_i} = \frac{F_i}{k_i} \quad (10)$$

where L_i , E_i , I_i are the length, Young's modulus, and area moment of inertia of the new elastic rod, respectively, and k_i is the equivalent flexural stiffness. To achieve a mapping of the mechanical properties between different elastic rods, we introduce a scaling coefficient k :

$$k = \frac{k_i}{k_r} = \frac{F_i u_r}{F_r u_i} \quad (11)$$

Using this scaling coefficient, the Force-Tactile signals \mathbf{X}_i of the new elastic rod can be equivalently mapped to the mechanical property distribution \mathbf{X}_r of the reference elastic rod:

$$\mathbf{X}_i = \frac{1}{k} \mathbf{X}_r, \quad \mathbf{X} \in \{F, T, H\} \quad (12)$$

In practical scenarios, when the robot interacts with a new elastic rod, the scaling coefficient k is first measured through simple experiments. Specifically, one end of both the reference rod and new elastic rod is fixed, and an identical force, perpendicular to the axis of the rods, is applied to the free ends. The displacements u_r and u_i at the tip of the reference and new rods, respectively, are measured, and the scaling coefficient is computed as $k = \frac{u_r}{u_i}$. Subsequently, the domain adapter utilizes this coefficient to scale the force, torque, and tactile signals from the new elastic rod. These scaled signals can be directly input into the pre-trained proactive motion planning model (see Fig. 3). The domain adapter enables the model to efficiently adapt to new soft objects with varying materials or shapes without requiring additional training, which significantly reduces the data acquisition and model training costs.

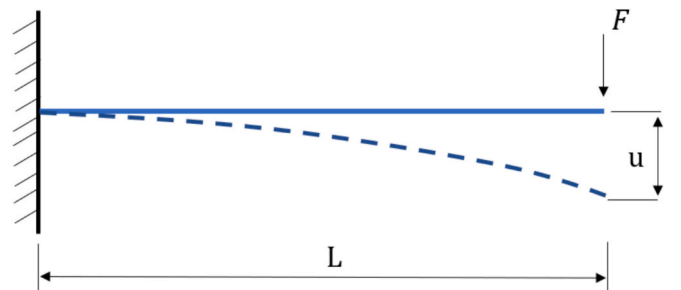


Fig. 4. Stress diagram of the elastic rod cantilever beam.

3.5. Adaptive admittance controller

To enhance the compliance and stability of human-robot collaboration, our approach also integrates a compliance control module. This module primarily achieves adaptive compliance control through a variable-parameter admittance controller. The admittance controller adjusts the robot's desired motion state in response to external forces, as represented by the following dynamic model of the standard admittance controller:

$$\mathbf{F}_{ext} = \mathbf{M}(\ddot{\mathbf{x}}_c - \ddot{\mathbf{x}}_t) + \mathbf{B}(\dot{\mathbf{x}}_c - \dot{\mathbf{x}}_t) + \mathbf{K}(\mathbf{x}_c - \mathbf{x}_t) \quad (13)$$

where \mathbf{F}_{ext} is the external force vector, \mathbf{M} is the inertia coefficient matrix, \mathbf{B} is the damping coefficient matrix, \mathbf{K} is the stiffness coefficient matrix. $\ddot{\mathbf{x}}_c$, $\dot{\mathbf{x}}_c$, \mathbf{x}_c , $\ddot{\mathbf{x}}_t$, $\dot{\mathbf{x}}_t$, \mathbf{x}_t represent the acceleration, velocity, and position vectors of the robot's desired trajectory and actual trajectory points, respectively. In human-robot collaborative transportation tasks, we aim for high compliance, meaning the robot should follow the operator's movements precisely while jointly manipulating the object. Such tasks require the robot to fully comply with the operator's actions. To achieve this, we set the stiffness matrix's diagonal elements to zero, thereby eliminating any restoring forces. Consequently, Equation (13) simplifies to:

$$\mathbf{F}_{ext} = \mathbf{M}(\ddot{\mathbf{x}}_c - \ddot{\mathbf{x}}_t) + \mathbf{B}(\dot{\mathbf{x}}_c - \dot{\mathbf{x}}_t) \quad (14)$$

The inertia matrix \mathbf{M} is a diagonal matrix representing the robot's inertia characteristics along each degree of freedom:

$$\mathbf{M} = \text{diag}(m_x, m_y, m_z, I_x, I_y, I_z) \quad (15)$$

where $m_x, m_y, m_z, I_x, I_y, I_z$ are the equivalent masses and equivalent rotational inertias along the x, y, and z axes, respectively. The damping matrix \mathbf{B} represents the system's damping characteristics, which are used to smooth the robot's motion. The diagonal elements represent the damping coefficients for each degree of freedom, while the off-diagonal elements represent the coupling effects between different degrees of freedom. We approximate \mathbf{B} as a diagonal matrix, which is a common strategy for computational simplicity [35].

$$\mathbf{B} = \text{diag}(b_x, b_y, b_z, b_{rx}, b_{ry}, b_{rz}) \quad (16)$$

where the diagonal elements correspond to the damping coefficients for the robot's end-effector translation and rotation along the x, y, and z axes. The adaptive admittance control model is proposed as follows:

$$\mathbf{B} = \max(0, \mathcal{F}(\xi, \delta)) \mathbf{B}_c + \mathbf{B}_e \quad (17)$$

$$\mathbf{M} = \omega_m \cdot \max(0, \mathcal{F}(\xi, \delta)) \mathbf{M}_c + \mathbf{M}_e \quad (18)$$

where,

$$\mathcal{F}(\xi, \delta) = \frac{1}{\Delta t} \left(\omega_1 \xi - \omega_2 \sum_{i=1}^n \int_t^{t+\Delta t} |\delta_i| dt \right) \quad (19)$$

$$\xi = \int_t^{t+\Delta t} \mathbb{I}(\dot{\mathbf{x}}_c(t) \cdot \dot{\mathbf{x}}_c(t - \epsilon) < 0) dt \quad (20)$$

In these equations, $\mathbf{B}_c, \mathbf{M}_c$ are the baseline damping and inertia matrices, and $\mathbf{B}_e, \mathbf{M}_e$ are constant matrices used to ensure the damping and inertia coefficients remain positive. The function $\mathcal{F}(\xi, \delta)$ is the adjustment function, where ξ represents the oscillation level of the robot's trajectory, measured by the number of oscillations of the robot's end-effector velocity within a unit time. The variable δ_i represents the deformation of the manipulated object in different directions. The indicator function \mathbb{I} ensures that ξ is calculated when the velocity oscillates, and $\omega_m, \omega_1, \omega_2$ are positive weighting coefficients. Δt is the time

window length, and ϵ is the time step length.

The weight adjustment function $\mathcal{F}(\xi, \delta)$ balances the stability and compliance of the robot's collaborative control. When ξ increases, indicating significant oscillations in the robot's end-effector motion, the diagonal elements of the inertia matrix \mathbf{M} and the damping matrix \mathbf{B} increase, thereby stabilizing the robot's response to external forces. Conversely, when ξ decreases, the diagonal elements of \mathbf{M} and \mathbf{B} decrease to improve compliance. Additionally, as δ_i increases, indicating greater deformation of the soft object, the diagonal elements of \mathbf{B}, \mathbf{M} decrease to enhance the robot's responsiveness to external forces, reducing the object's deformation. This formulation extends conventional admittance control by introducing an adaptive parameter tuning mechanism based on the system's oscillation and object deformation, allowing the robot to dynamically adapt to varying interaction conditions in human-robot collaboration.

The adaptive admittance controller works in tandem with the proactive motion planning module. The controller uses the predicted object deformation information and external force data from the motion planning module to adaptively adjust the admittance parameters, thereby providing high-frequency compliance control.

4. Experiments and results

4.1. Experiment settings

To validate the proposed approach, we conducted a series of experiments. Fig. 5(a) and 5(b) illustrate the experimental setups for the rail-robot and human-robot collaborative transportation scenarios, respectively. In the rail-robot scenario, routine rail motion is employed to ensure a fair comparison of the method's performance between different methods, while the human-robot scenario tests the effectiveness of the proposed approach in real human-robot handling context. The experiment utilizes a 6-DOF multi-joint robot arm (JAKA Zu3), which is mounted on an aluminum alloy frame. A Robotiq 2F-85 gripper is attached to the robot, and a dual-DOF linear rail is placed on the table. The rail's slider is equipped with a rotatable platform, allowing for both x,y axes translation and z axis rotation, thereby simulating human hand's holding movements. One end of a silicone rod (with a Shore hardness of 55A, length of 50 cm, diameter of 35 mm) is grasped by the robot's gripper, while the other end is either held by a clamp on the rotatable platform (Fig. 5(a)) or by a human hand (Fig. 5(b)).

To collect real-time data during the collaborative handling process, we use both F/T sensors and tactile sensors. The F/T sensor (JK-SE-II-200) is mounted on the wrist joint of the robot, and two PapillArray Tactile Sensor arrays are installed on the inner sides of the gripper fingers, measuring the 3-axes force at 9 contact points on each side, as shown in Fig. 5(a). All algorithmic models were executed on a workstation equipped with an Intel Core i7-12700F CPU, 16 GB of RAM, and an NVIDIA RTX 3080 GPU. The neural network components were developed and trained using Python within the PyCharm environment. Meanwhile, the real-time robot control modules were implemented in C#, and the low-level robot control was enabled through the official SDK provided by JAKA Robotics. The entire system was deployed on a Windows 10 platform. Communication between the Python and C# modules was established via TCP/IP sockets to ensure efficient data exchange during real-time collaborative execution.

The experiments are designed as follows: In Sec. 4.2, we evaluate the accuracy of the deformation prediction model based on multi-modal state representation. In Sec. 4.3, we compare the performance of the proactive motion planning module with ablation methods in a virtual environment to evaluate its effectiveness. Section 4.4 presents ablation and comparative tests conducted in the rail-robot scenario to examine the performance of our proposed HRCT method in physical environment. Finally, in Sec. 4.5, human-robot collaborative experiments are conducted and the generalization ability of the proposed method across different object stiffness and collaboration tasks is demonstrated.

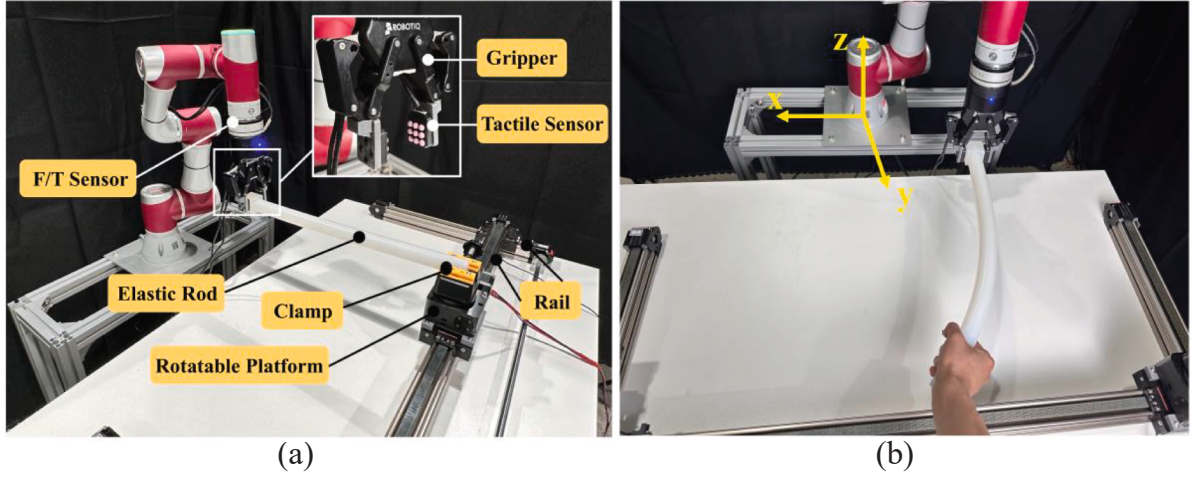


Fig. 5. Experiment settings. (a) Rail-robot transportation settings. (b) Human-robot transportation settings.

4.2. Evaluation of the multi-modal encoder and deformation prediction model

We first pretrained the multi-modal encoder and deformation prediction model to support the subsequent training of the motion planning model. To reduce the cost of data collection, we use a rail-slider system to simulate various hand grasp positions and automatically collect F/T data ($\mathbf{F} = (F_x, F_y, F_z)$, $\mathbf{T} = (T_x, T_y, T_z)$) and tactile signals \mathbf{H} , as shown in Fig. 6(a). To capture accurate deformation information of the soft rod, four strain gauges (BF 120–50 AA) are attached to the midpoint of the rod surface to measure deformation in four directions, as depicted in Fig. 6(b). During the experiment, the rail slider and robot move randomly within the relative deviation ranges: $\Delta x \in [-50, 50]$ mm, $\Delta y \in [-10, 10]$ mm, $\Delta \theta \in [-15, 15]^\circ$. A total of 10 thousand measurement samples from various positions were collected, which took approximately 8 h. To prevent residual stress in the tactile sensors due to relative slippage between the soft rod and the gripper, a grasp initialization process is implemented. Specifically, after collecting every 20 samples, the gripper releases and re-grips the soft rod, and the tactile sensors are recalibrated for eliminating any bias.

We compare our method (referred to as Tactile (CNN) + F/T(MLP)) with four ablation methods, as summarized in Table 1. All methods utilize an encoder-decoder architecture, where the encoder processes F/T or tactile data and output a 32-dimensional latent vector. The decoder network (see Fig. 2) remains consistent across all methods which receives the latent vector and predicts the deformation value. Specifically,

Table 1

Settings and performance of encoder-decoder methods. The bolded numbers represent the best performance. * indicates our proposed method.

Method	Sensor		Tactile Network		Train Loss	Test Loss	Prediction Error
	Tactile	F/T	CNN	MLP			
Tactile (CNN) + F/T (MLP)*	✓	✓	✓		0.008	0.011	10.6 %
Tactile (MLP) + F/T (MLP)	✓	✓		✓	0.009	0.013	11.2 %
Tactile (MLP)	✓			✓	0.012	0.015	12.2 %
Tactile (CNN)	✓		✓		0.011	0.014	11.5 %
F/T (MLP)		✓			0.016	0.020	14.1 %

our proposed method employs CNN and MLP networks to encode the tactile and F/T data. The Tactile (MLP) + F/T(MLP) method uses MLP networks to encode both the tactile and F/T data, with the F/T network being identical to our method. In contrast, the tactile network directly concatenates the raw tactile data and inputs it into a 3-layer MLP with 64 hidden units to generate a 16-dimensional latent vector. The Tactile

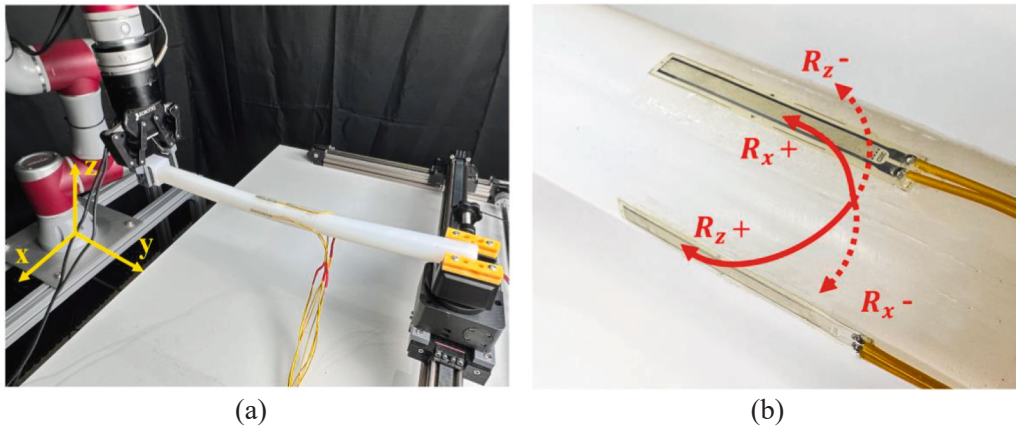


Fig. 6. Experiment setup for data collection. (a) The rail-robot system for multi-modal data collection. (b) Strain gauges are attached to the soft rod for measuring deformation in four directions (positive/negative bending around x and z axes).

(MLP) method only employs a 3-layer MLP network with 64 units to encode tactile data. The Tactile (CNN) method uses a CNN to encode tactile data, with the network architecture being identical to our approach. Finally, the F/T(MLP) method encodes the F/T data using an MLP network, similar to the MLP network used in our method.

The representation encoder and deformation prediction model are trained jointly, with the loss function being the mean squared error (MSE) of the deformation prediction. All methods are trained under the same hyperparameter settings: learning rate = 0.0001, batch size = 32, using the Adam optimizer, for 200 epochs.

Table 1 also lists the training loss, test loss, and deformation prediction error for each method. we can observe that the proposed Tactile (CNN) + F/T(MLP) method exhibits the smallest training loss, test loss, and prediction error, demonstrating the best performance in deformation prediction. Compared to single-modal methods (i.e., Tactile (MLP), Tactile (CNN), F/T(MLP)), the use of multi-modal methods (i.e., Tactile (CNN) + F/T(MLP), Tactile (MLP) + F/T(MLP)) reduces the deformation prediction error. This is likely due to the complementary nature of tactile and F/T data, with tactile data reflecting local features of the contact area, while F/T data represents the overall force state of the human-robot system. By integrating these two types of data, our model gains a more comprehensive understanding of the object's contact state and deformation characteristics, thereby enhancing both state representation and deformation prediction. Additionally, when selecting the tactile encoder, the CNN architecture outperforms the MLP network in terms of prediction accuracy. This is potentially because tactile data contains rich spatial features, and CNNs are better suited to exploit the spatial correlations in tactile data, efficiently extracting deformation characteristics of the target object. In contrast, MLP may be not good at handling high-dimensional complex data with spatial dependencies.

It is worth noting that strain gauges are only used during the offline data collection phase to label ground-truth deformation, and are not required during actual task execution. Based on additional experiments, the placement location of strain gauges during training has trivial impact on final task performance. For practical deployment, we recommend placing the strain gauges near the midpoint of the reference object, as this region tends to provide more stable deformation data while simplifying installation.

4.3. Validation of the robot motion planning model

Since Unity cannot simulate force and tactile sensors with high precision, we first pretrained a Force-Tactile Predictor to generate simulated F/T and tactile data to support the RL-based motion planning. The Force-Tactile Predictor is a 4-layer MLP network, with each layer consisting of 128 neurons as shown in Sec 3.3. The input consists of the relative position differences between the robot's end-effector and the slider's end ($\Delta x, \Delta y, \Delta \theta$), where $\Delta x = x_{robot} - x_{slider}$, $\Delta y = y_{robot} - y_{slider}$, $\Delta \theta = \theta_{robot} - \theta_{slider}$, and the output is the predicted tactile data and F/T data. The training data is sourced from the data collected in Section 4.2, and the training loss is the mean squared error (MSE) between the predicted and actual F/T and tactile data. The model is trained with a learning rate of 0.0001, a batch size of 32, and the Adam optimizer for 200 epochs. The test results show that the F/T prediction error is 3.7 %, and the tactile prediction error is 5.1 %, which demonstrate the high accuracy of the pretrained Force-Tactile Predictor.

After obtaining the pretrained representation encoder, deformation prediction model, and the Force-Tactile predictor, we proceed to train the RL-based robot motion planning model in the Unity environment. As shown in Fig. 7, we first construct a rail-robot model in Unity, where the slider can move along the x and y axes and rotate around the z-axis on the rail. The slider's movement range is: $x_{slider} \in [-25, 25]$ cm, $y_{slider} \in [-5, 5]$ cm, $\theta_{slider} \in [-20, 20]^\circ$, with random movement velocities: $v_x \in [-5, 5]$ cm/s, $v_y \in [-0.5, 0.5]$ cm/s, $\omega \in [-2, 2]^\circ$ /s. The RL agent's action velocity range matches that of the slider. The reward

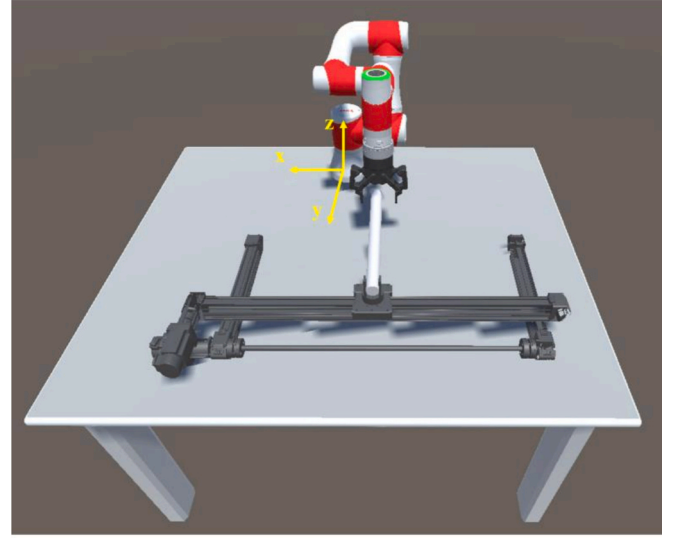


Fig. 7. The RL-based robot motion planning model training in Unity environment.

function parameters for Equations (3)-(5) are set as follows: $\lambda_1 = 0.01$, $\lambda_2 = 0.001$, $C_{max} = 200$, $\sigma_x = 5$ cm, $\sigma_y = 2$ cm, $\sigma_\theta = 24^\circ$.

We utilized the five pretrained representation encoders and deformation prediction models from Section 4.2 to generate latent vectors as the state input for the RL model and to predict the deformation of soft rod. Each RL model was trained for 5 million steps, with each training process taking approximately 2 h. The cumulative reward curves of these five RL models are shown in Fig. 8. As observed, the proposed Tactile (CNN) + F/T(MLP) method yields the highest cumulative reward. Moreover, the multi-modal methods significantly outperform the single modal methods in terms of reward. This may be because combining tactile and F/T information provides a more comprehensive state representation, mitigating the influence of data noise or information gaps (e.g., the lack of detailed local contact information for F/T sensors, the lack of comprehensive global force data for tactile sensors) that might arise from using a single modality. This helps the RL model learn a more optimal motion policy. Furthermore, a more accurate deformation prediction model further enhances the performance of the RL model.

To further evaluate the model's performance, we conducted 1,000 test runs for each of the five methods in the virtual environment, with the results shown in Table 2. The performance metrics include task success rate (i.e., the percentage of episodes where the relative distance between the robot and slider remains within a predefined range), and translational following errors along the x, y axes, as well as rotational following errors around z-axis. As seen in Table 2, the proposed method outperforms all other models across all metrics, achieving a task success rate of 99.8 % with following errors of 9.4 mm, 1.9 mm, and 3.2° in the x, y, and z axes, respectively. In contrast, the F/T(MLP) method performs the worst, with a success rate of 93.1 %, and the largest following errors in all directions (22.1 mm, 3.9 mm, and 11.2° , respectively). This may be due to the fact that F/T data struggles to effectively capture local contact states and complex soft contact dynamics, leading to insufficient state representation. For the Tactile (MLP) and Tactile (CNN) methods, their success rates and following errors are better than those of the F/T(MLP) method, likely because tactile data captures local contact information, which is crucial for human-robot collaborative manipulation of soft targets. However, their performance still lags that of the multi-modal fusion methods, since the multi-modal models fully exploit the complementary advantages of tactile and F/T data, leading to enhanced state representation. Tactile data provides fine-grained contact deformation information, especially in scenarios involving complex local contact,

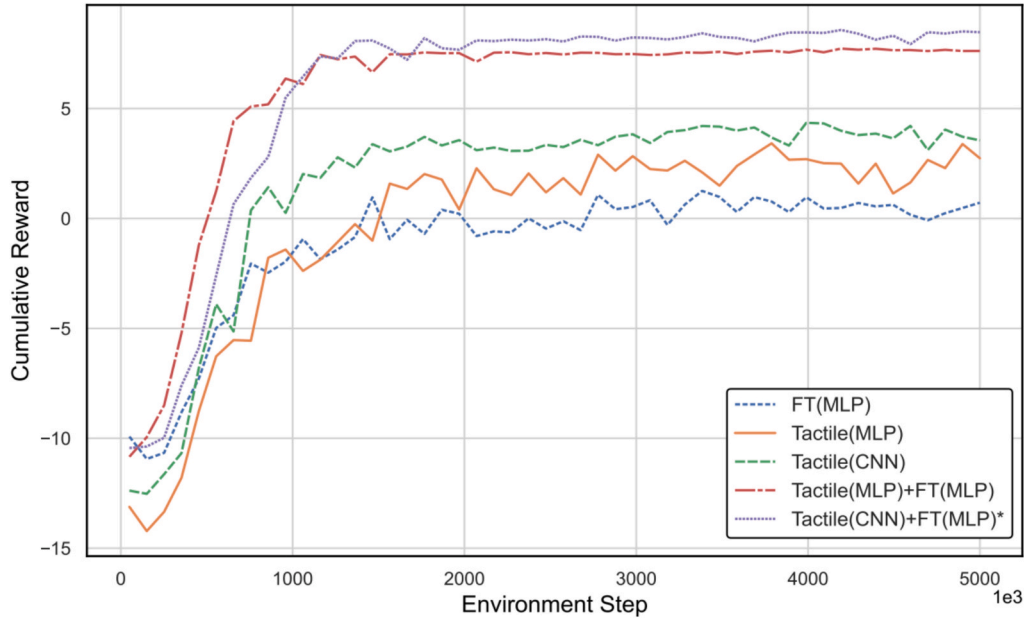


Fig. 8. Cumulative reward curve of different RL models.

Table 2

Task success rate and following deviation of different methods. The bolded numbers represent the best performance. * indicates our proposed method.

Method	Success Rate	Following Deviation		
		$e_x(mm)$	$e_y(mm)$	$e_\theta(^{\circ})$
Tactile (CNN) + F/T (MLP)*	99.8 %	9.4	1.9	3.2
Tactile (MLP) + F/T (MLP)	98.5 %	11.6	2.1	6.4
Tactile (MLP)	94.7 %	19.7	3.3	9.4
Tactile (CNN)	96.4 %	13.5	2.4	7.3
F/T (MLP)	93.1 %	22.1	3.9	11.2

helping more precisely adjust the robot's local movement. On the other hand, F/T data offers global force balance and dynamic force variation information, assisting in maintaining stability during large-range movements. By combining tactile and F/T data, the multi-modal approach achieves comprehensive perception of both local and global contact states, resulting in higher task success rates and smaller following errors in handling soft-object tasks.

4.4. Rail-robot transportation performance

In this section, we compare our proposed Collaborative Deformable-Object Transportation (CoDoT) method with five ablation methods, as well as two state-of-the-art methods, ACC [23] and AIC [35] (as shown in Table 3) in the rail-robot scenario. We fixed one end of the elastic rod to the rail slider to generate the routine movement patterns, which

Table 3

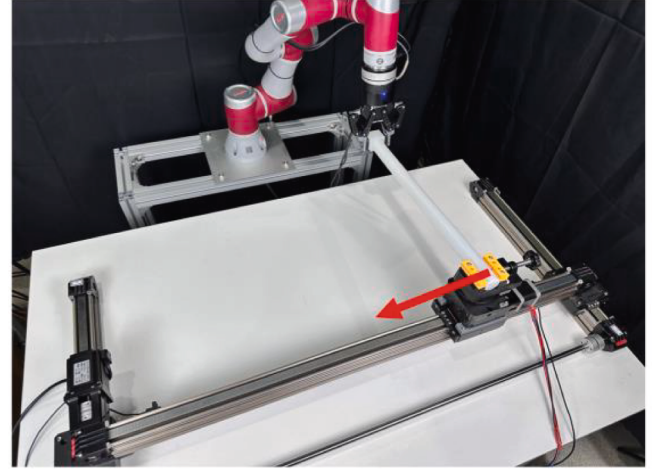
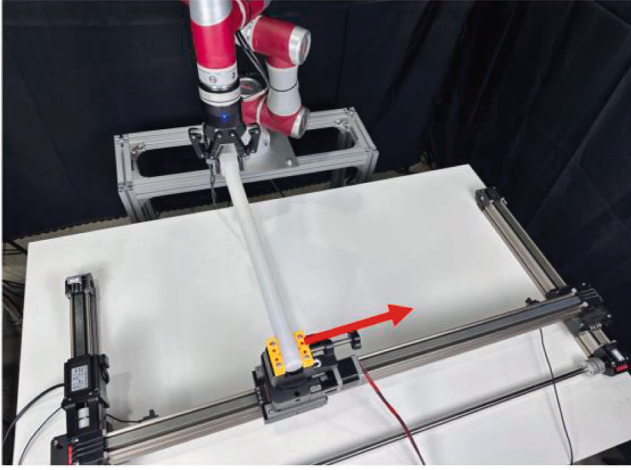
Settings of ablation and compared methods. * indicates our proposed method.

Method	Admittance Controller		Proactive Decision Model
	Fixed	Adaptive	
CoDoT*		✓	F/T + Tactile
CoDoT (Tac)		✓	Tactile
CoDoT (F/T)		✓	F/T
RLDoT			F/T + Tactile
Var-Ad		✓	
Fixed-Ad	✓		
ACC [23]	✓		
AIC [35]		✓	Human-robot Motion

ensures a fair comparison between our method and other approaches. Our proposed CoDoT is a hybrid control method that combines a multi-modal state representation-based motion planning module with an adaptive admittance controller. The parameters of the admittance controller are set as follows: weighting coefficients are $\omega_m = 0.8$, $\omega_1 = 10$, $\omega_2 = 0.25$, time window length $\Delta t = 1000ms$, time step length $\epsilon = 20ms$, baseline and constant inertia matrices $\mathbf{M}_c = \text{diag}(1.5, 1.5, 1.5, 0.3, 0.3, 0.3)$, $\mathbf{M}_e = \text{diag}(0.5, 0.5, 0.5, 0.1, 0.1, 0.1)$, baseline and constant damping matrices $\mathbf{B}_c = \text{diag}(20, 20, 20, 3, 3, 3)$, $\mathbf{B}_e = \text{diag}(3, 3, 3, 0.5, 0.5, 0.5)$. These parameters were chosen based on prior controller tuning experience and validated to ensure stable and responsive compliant motion in the collaborative tasks. The ablation methods CoDoT (Tac) and CoDoT (F/T) are also hybrid control models that utilize motion planning modules based on single-modal (Tactile or F/T) state representations combined with an adaptive admittance controller. RLDoT is an active control model that solely relies on a multi-modal state representation-based motion planning module. Var-Ad and Fixed-Ad are compliant control methods, with the former only using the adaptive admittance controller and the latter employing a fixed-parameter admittance controller. ACC is an advanced hybrid control approach that dynamically adjusts the robot's motion by introducing an adaptive exponent based on the operator hand's velocity and admittance reference velocity, combined with a fixed-parameter admittance controller for collaborative control. The AIC method adapts the impedance controller by adjusting the impedance parameter weight function based on the relative position of the robot and human hand. We conduct 10 tests in each of the following three manipulation scenarios: 1D Linear motion, 2D Linear motion, and Zigzag motion.

(1) 1D Linear motion task

The 1D Linear motion task scenario is shown in Fig. 9(a), where the rail slider undergoes back and forth translational movements along the x-axis with a one-way travel distance of 50 cm and speed of $v_x = 5 \text{ cm/s}$. The performance metrics for the task include the average deformation of the elastic rod, $\delta = \frac{1}{4} \sum_{i=1}^4 |\delta_i|$, where δ_i is the deformation measured by the four strain gauges. Additionally, the following deviation metrics are measured: the x-axis and y-axis following deviations between the robot and the slider, $e_x = x_{\text{robot}} - x_{\text{slider}}$, $e_y = y_{\text{robot}} - y_{\text{slider}}$, respectively. For clearer performance comparisons, all methods are categorized into three



(a) 1D Linear Motion

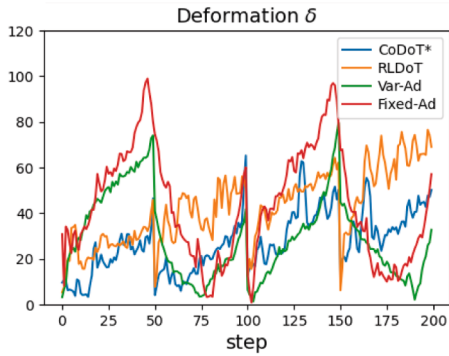
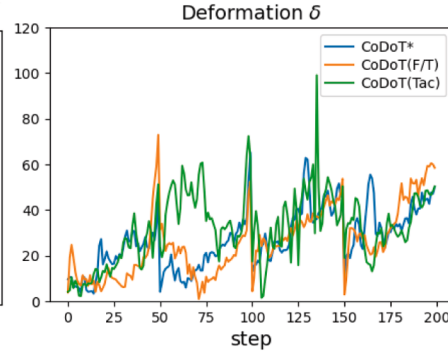
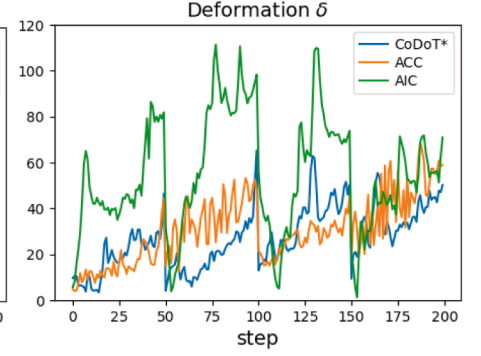
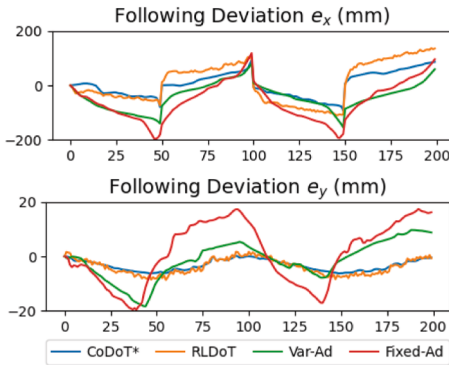
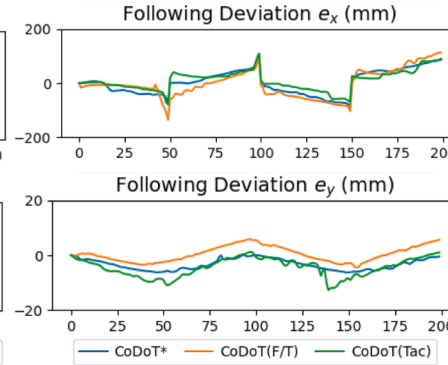
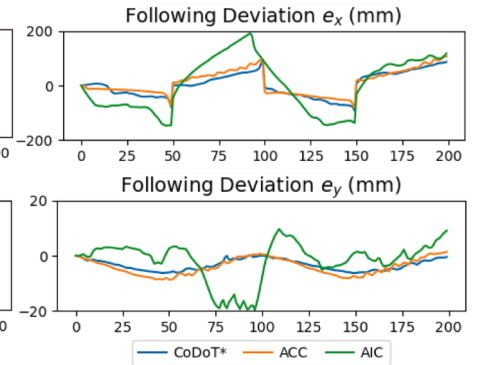
(b) δ : Group 1(c) δ : Group 2(d) δ : Group 3(e) e_x, e_y : Group 1(f) e_x, e_y : Group 2(g) e_x, e_y : Group 3

Fig. 9. Performance comparison in 1D Linear motion task.

groups. Group (1) includes CoDoT, RLDiT, Var-Ad, and Fixed-Ad, and is used to ablate and compare the effects of the compliance control module, the proactive motion planning module, and the variable admittance controller. Group (2) consists of CoDoT, CoDoT (F/T), and CoDoT (Tac), which are used to compare the performance of multi-modal sensors against single-modal sensors. Group (3) includes CoDoT, ACC, and AIC, and is aimed at comparing our method with other state-of-the-art approaches.

Fig. 9 (b)-(g) show the performance comparisons for these methods. It is evident that the proposed hybrid control method (CoDoT) outperforms all other methods in terms of both the overall deformation δ

and the following deviations e_x, e_y . When proactive motion planning is employed but without adaptive compliance control, the RLDiT method exhibits larger fluctuations in the following deviations. This may be due to that when only relying on proactive motion planning control, the robot becomes more sensitive to changes in external forces, leading to motion instability. On the other hand, when adaptive compliance control is used but without proactive motion planning, the Var-Ad method leads to larger deformation of the target object. This is likely because compliance control cannot predict changes in human-robot collaboration tasks, especially when the slider changes its direction of movement (e.g., steps 50, 100, and 150). In such cases, the robot fails to respond

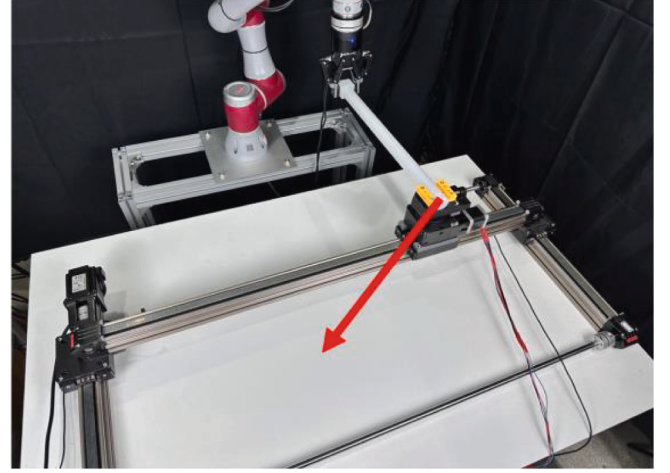
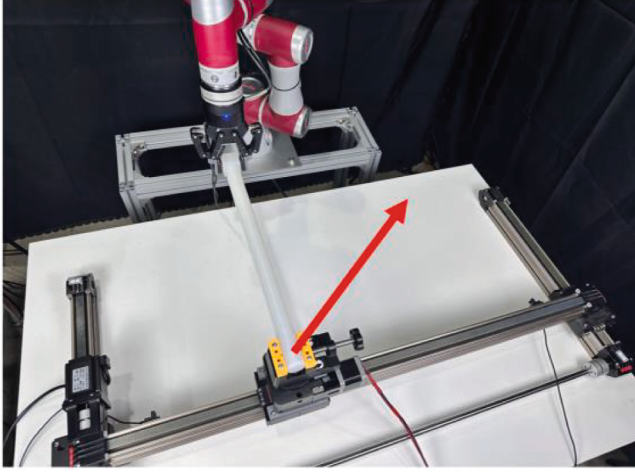
with precise movements, causing significant deformation of the target object. In contrast, the proposed CoDoT method results in minimal and smooth changes in both target deformation and following deviation, demonstrating its stability to external motion changes and disturbances.

Additionally, the Fixed-Ad method performs the worst in terms of both object deformation and following deviations. This may be due to the fixed admittance control parameters, which are unable to adapt to dynamic environmental changes, thus preventing dynamic adjustment for compliance control. Besides, from Fig. 9 (c) and (f), we observe that when only single-modal state representation models are used, the object deformation and collaborative following deviations increase for both

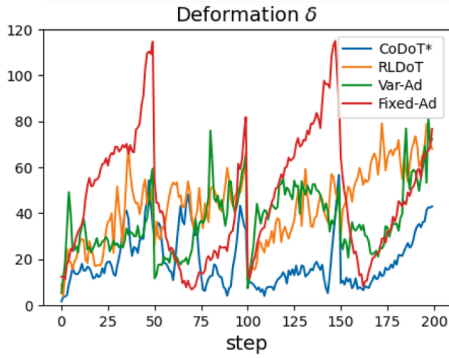
CoDoT (F/T) and CoDoT (Tac). This suggests that single-modal tactile or F/T information is insufficient to fully and accurately represent the collaborative manipulation state, leading to control strategies that are unable to adapt accurately to the movement of the rail slider.

(2) 2D Linear motion task

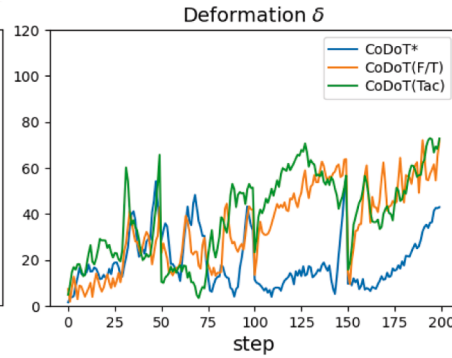
The 2D Linear motion task scenario is depicted in Fig. 10(a), where the rail slider undergoes reciprocal translational movements along both the x-axis and y-axis. The movement distances along the x-axis and y-axis are 50 cm and 30 cm, respectively, with slider velocities of $v_x =$



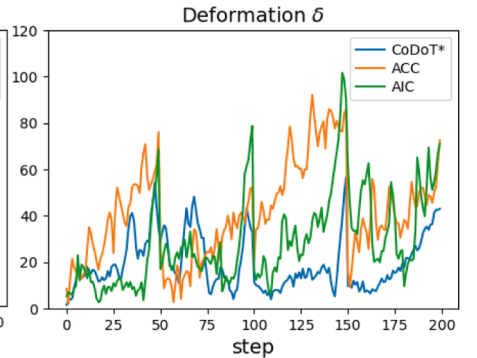
(a) 2D Linear Motion



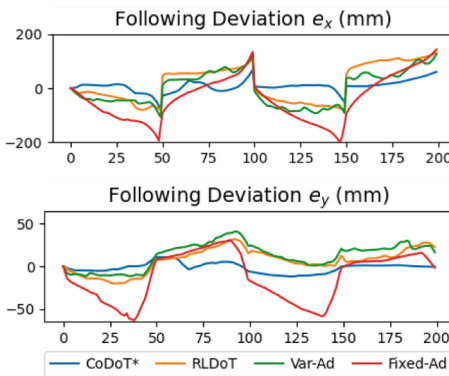
(b) δ : Group 1



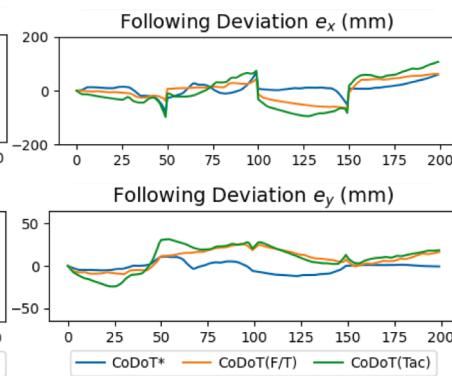
(c) δ : Group 2



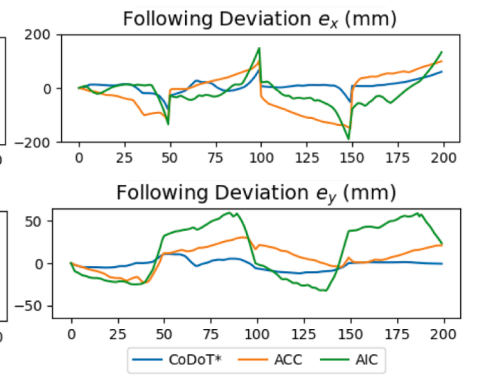
(d) δ : Group 3



(e) e_x, e_y : Group 1



(f) e_x, e_y : Group 2



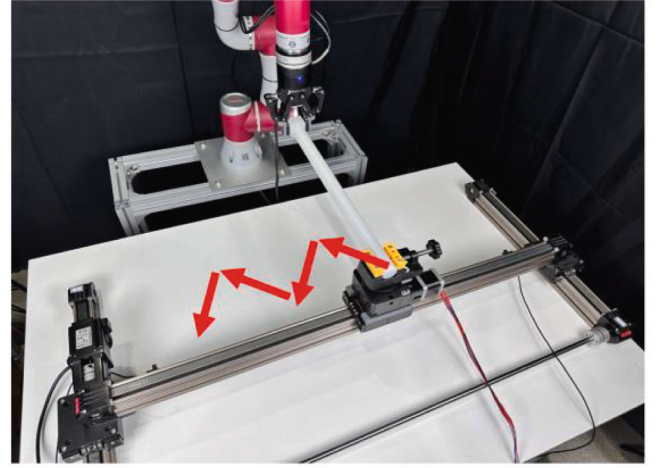
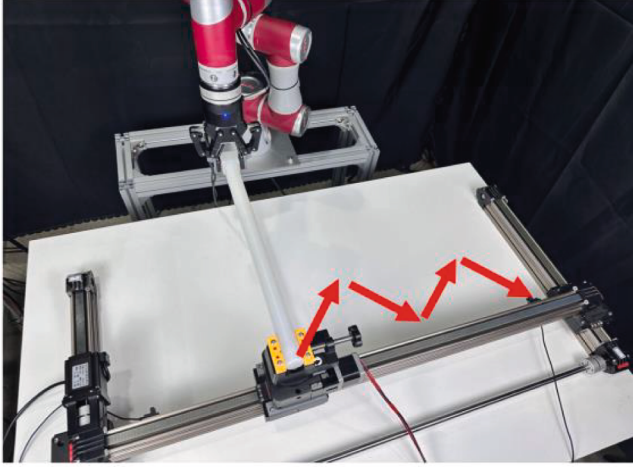
(g) e_x, e_y : Group 3

Fig. 10. Performance comparison in 2D Linear motion task.

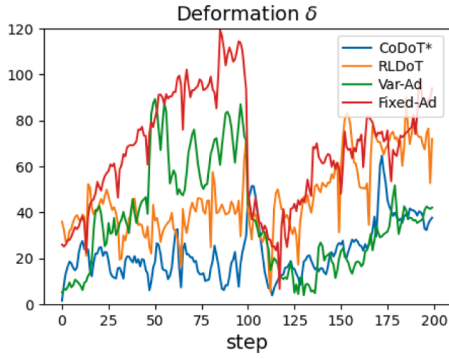
5 cm/s, $v_y = 3$ cm/s. Fig. 10(b)-(g) show the performance of the 2D Linear motion task, revealing that the proposed CoDoT method excels in both target object's deformation and following deviations. Specifically, the maximum target deformation of CoDoT is 56, which represents a 22.2 % improvement compared to the second-best method CoDoT (Tac) (with a maximum deformation of 72). Additionally, the maximum following deviations of CoDoT along the x-axis and y-axis are 79 mm and 12 mm, respectively. In comparison, the CoDoT (F/T) method achieves maximum deviations of 84 mm and 26 mm. This result indicates a clear improvement in y-axis following performance of CoDoT, with a reduction of 53.8 % in following deviation compared to CoDoT(F/T).

(3) Zigzag motion task

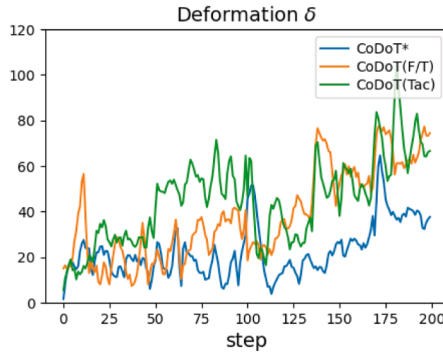
The Zigzag motion scenario is shown in Fig. 11(a) which involves the rail slider performing zigzag-type reciprocal translational movements along with the x-axis and y-axis. The one-way movement distances for the x-axis and y-axis are 50 cm and 10 cm, respectively, with velocities $v_x = 5$ cm/s, $v_y = 4$ cm/s. In this task, the frequent change of slider motion direction significantly increases the system fluctuations, placing larger challenges on the collaborative performance. The experiment results are shown in Fig. 11(b)-(g). We can see that the proposed CoDoT method continues to demonstrate superior performance in both target



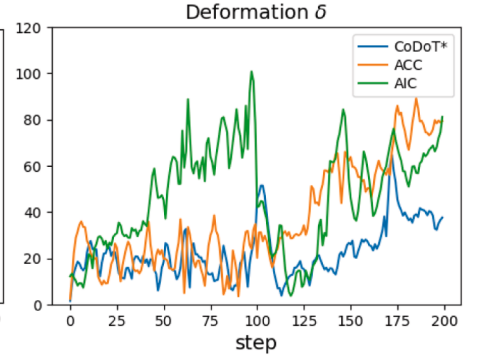
(a) Zigzag Motion



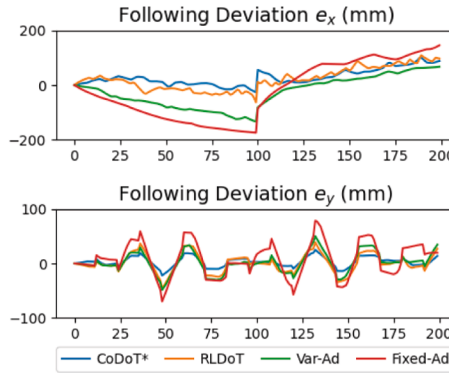
(b) δ : Group 1



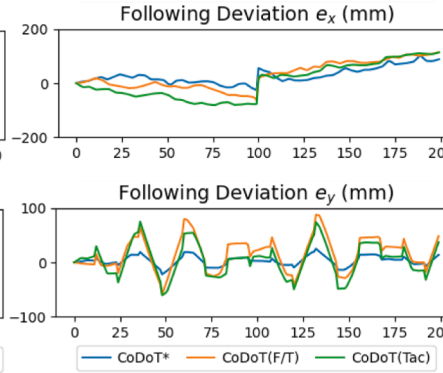
(c) δ : Group 2



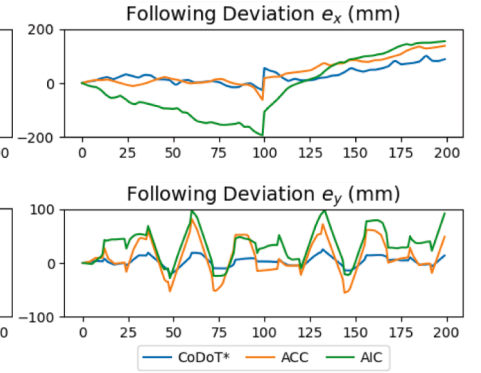
(d) δ : Group 3



(e) e_x, e_y : Group 1



(f) e_x, e_y : Group 2



(g) e_x, e_y : Group 3

Fig. 11. Performance comparison in Zigzag motion task.

deformation control and following deviation. Specifically, the maximum deformation for the CoDoT method is 64, which is a 17 % reduction compared to the second-best CoDoT(F/T) method (with a maximum deformation of 77). This highlights the significant advantage of CoDoT in deformation control. Moreover, the following deviations for CoDoT remain within a smaller range compared to other methods. The following deviation fluctuations are notably reduced, particularly along the y-axis, where CoDoT effectively suppresses the magnitude and abrupt changes of deviation fluctuations. In contrast, the y-axis following deviations of other methods exhibit larger fluctuations and instability. These results indicate that the proposed CoDoT method is capable of maintaining stable collaborative performance in complex and rapidly changing motion scenarios, demonstrating its reliability and superiority in dynamic environments.

Additionally, we conducted a comparison of the normalized soft rod deformation and the average force exerted on the robot end-effector ($F = \frac{1}{3}(|F_x| + |F_y| + |F_z|)$), with the detailed results shown in Table 4. As observed, the CoDoT method exhibits the least deformation across all tasks, demonstrating the superior following performance and the ability to maintain target shape stability in these collaborative handling scenarios.

Regarding the force exerted on the robot, CoDoT shows the lowest forces in Task 1 and Task 2 (1.45 N and 2.12 N, respectively). In Task 3, the force is 3.35 N, which is second only to the CoDoT (F/T) method, which records a force of 3.32 N. These results highlight the collaborative compliance advantage of the proposed method, where the operator only needs to apply small force to successfully cooperate with the robot in the handling tasks. In contrast, when only the adaptive admittance controller (Var-Ad) or the proactive model (RLDoT) is used, both deformation and force metrics perform worse, illustrating the limitations of solely relying on either adaptive compliance or proactive control. Furthermore, the performance of Var-Ad is significantly better than Fixed-Ad. This can be attributed to the adaptive nature of the admittance controller, which adjusts damping and inertial coefficients based on the target deformation level. When deformation increases (primarily due to the robot's position lagging behind the slider), the adaptive admittance controller reduces the damping and inertial coefficients, enhancing force-controlled compliance and enabling the robot to follow the slider movement more effectively, thus reducing target deformation. Compared to the single-modal hybrid collaboration methods, such as CoDoT(F/T) and CoDoT (Tac), the proposed CoDoT method achieves better deformation control while also showing competitive force metrics. This demonstrates the value of utilizing both tactile and F/T information in soft-object collaborative transportation tasks. While CoDoT achieves the lowest deformation across all tasks, its performance in Task 1 is slightly worse than in Tasks 2 and 3. This may be resulted by a

combination of factors: the soft rod's greater susceptibility to lateral bending under x-axis motion (dominant in Task 1), localized stress concentration from the rail-slider's rigid clamping, and CoDoT's ability to suppress oscillations, which reduces object deformation in more complex trajectories in Task 3. It is worth noting that Table 4 is intended to compare the performance of different methods under the same task settings, rather than to analyze the relative difficulty or deformation severity across tasks.

In summary, the proposed CoDoT method performs the best in deformation control across all handling scenarios, while also exhibiting excellent performance in the average force exerted on the robot with outstanding compliance and stability.

4.5. Human-robot transportation task

4.5.1. Evaluation on benchmark silicon rod

To further evaluate the practical performance of the proposed method, we conducted comparison experiments in real human-robot collaboration scenarios. The experiments were carried out in three scenarios (1D Linear motion, 2D Linear motion, and Zigzag motion) similarly as we did in Sec. 4.4, with ten tests for each scenario. Experiment results are presented in Fig. 12 and Table 5. Considering the challenges associated with accurately tracking hand position in dynamic human-robot collaboration scenarios, we focus on evaluation metrics such as object deformation, average force exerted on the robot, and subjective ratings from the human participants, which are more directly related to the task performance and user experience. We recruited 10 participants to complete the three collaborative handling tasks. The evaluation criteria were adapted from previous work [38] and consisted of three dimensions: Smoothness (measuring the operational fluidity of the participants), Task Ease (assessing how easy the participants feel, including whether the robot's response matches with their expectations and the physical effort required), and Response Speed (evaluating the speed with which the robot adjusted to the human hand's movements). Each metric was rated on a scale of 0 to 10, with higher scores indicating better performance.

As shown in Fig. 12(d)-(l), compared to the rail-robot scenario, the object deformation for all methods were reduced in human-robot scenario. This change is mainly attributed to that in the rail-robot scenario, the soft rod is tightly clamped to the slider, causing stress concentration and thus increasing both force and deformation. In contrast, in the human-robot scenario, the human hand's grip, characterized by a more even contact distribution and softer contact, reduces stress concentration on the soft rod, thereby effectively alleviating deformation. Additionally, the proposed CoDoT method exhibited the lowest target deformation across all motion scenarios, with the maximum deformation values of 27, 33, and 47, respectively. Compared to the second-best method, RLDoT (with maximum deformations of 37, 40, and 61, respectively), our method achieved 27.0 %, 17.5 %, and 23.0 % in deformation reductions, demonstrating its strong capability in controlling target deformation across different human-robot motion scenarios. These results reflect the excellent collaborative performance of the proposed method. Furthermore, CoDoT exhibited the smallest fluctuations in target deformation and the lowest deformation range across the tasks, highlighting its adaptability and stability to different human motion states.

From Table 5, we can observe that the CoDoT method outperforms all other methods in object deformation and exerted force across all tasks, with soft rod deformation ranging from 0.13 to 0.25 and exerted force ranging from 1.75 N to 2.07 N. Regarding user ratings in the human-robot collaboration tasks, CoDoT achieved the highest scores in all three dimensions: 9.3 for Smoothness, 9.7 for Task Ease, and 8.8 for Response Speed. Among the tested methods, RLDoT performed the worst in Smoothness. This could be due to its reliance on multi-sensor data and complex reasoning, leading to communication delays and low control frequency, which caused discontinuous robot movements

Table 4

Performance of different methods on three tasks in rail-robot experiments. Bolded numbers represent the best performance. * indicates our proposed method.

Method	Normalized Object Deformation (0 ~ 1)			Average Exerted Force (N)		
	Task 1 (1D Linear)	Task 2 (2D Linear)	Task 3 (Zigzag)	Task 1 (1D Linear)	Task 2 (2D Linear)	Task 3 (Zigzag)
CoDoT*	0.26	0.19	0.23	1.45	2.12	3.35
CoDoT (Tac)	0.32	0.39	0.38	1.85	3.62	3.54
CoDoT (F/T)	0.27	0.34	0.35	1.73	2.76	3.32
RLDoT	0.42	0.43	0.46	3.74	4.25	6.22
Var-Ad	0.29	0.37	0.41	2.23	3.79	5.37
Fixed-Ad	0.52	0.47	0.58	5.94	5.58	6.34
ACC [23]	0.33	0.35	0.37	2.03	3.78	3.63
AIC [35]	0.41	0.31	0.42	3.76	4.03	4.59

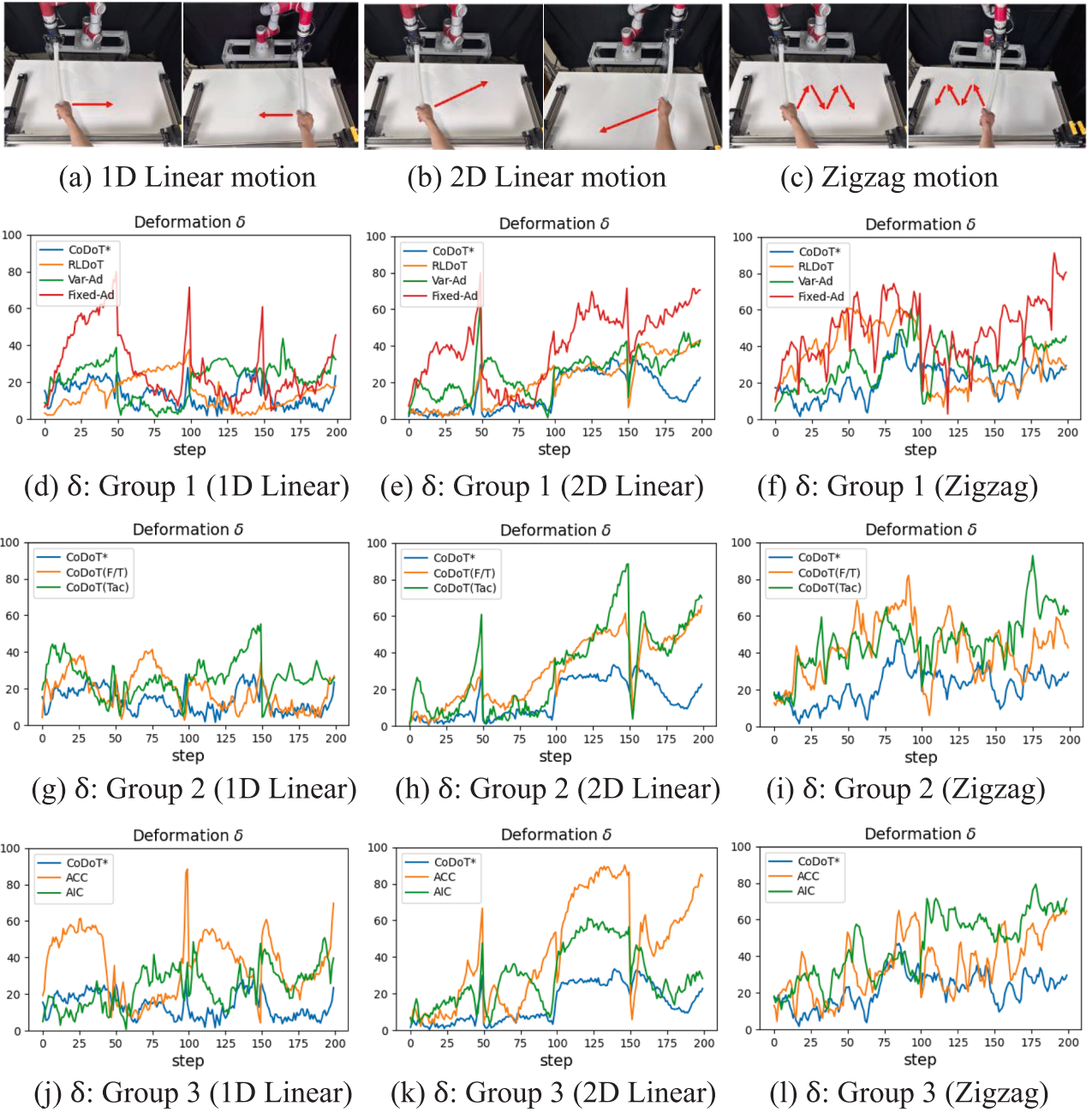


Fig. 12. Performance comparison in real human-robot collaboration scenarios.

Table 5

Performance of different methods on three tasks in the human-robot scenario experiments. Bolded numbers represent the best performance. * indicates our proposed method. (Higher values of participant ratings reflect better human-robot collaboration performance.).

Method	Normalized Object Deformation (0 ~ 1)			Average Exerted Force (N)			Participant Ratings (0 ~ 10)		
	Task 1 (1D Linear)	Task 2 (2D Linear)	Task 3 (Zigzag)	Task 1 (1D Linear)	Task 2 (2D Linear)	Task 3 (Zigzag)	Smoothness	Task Ease	Response Speed
CoDoT*	0.13	0.18	0.25	1.98	1.75	2.07	9.3	9.7	8.8
CoDoT (Tac)	0.23	0.25	0.36	2.63	1.93	2.32	9.0	8.5	8.6
CoDoT (F/T)	0.18	0.28	0.31	2.45	1.89	2.14	8.9	9.0	8.7
RLDoT	0.16	0.21	0.33	2.86	2.22	3.50	6.1	7.0	6.8
Var-Ad	0.21	0.25	0.35	2.94	2.82	3.41	8.0	5.2	6.9
Fixed-Ad	0.39	0.44	0.49	6.11	6.73	6.90	7.2	3.7	5.5
ACC [23]	0.28	0.38	0.31	3.74	3.99	3.27	8.7	9.0	8.5
AIC [35]	0.24	0.31	0.34	3.56	2.61	3.67	8.4	7.9	6.4

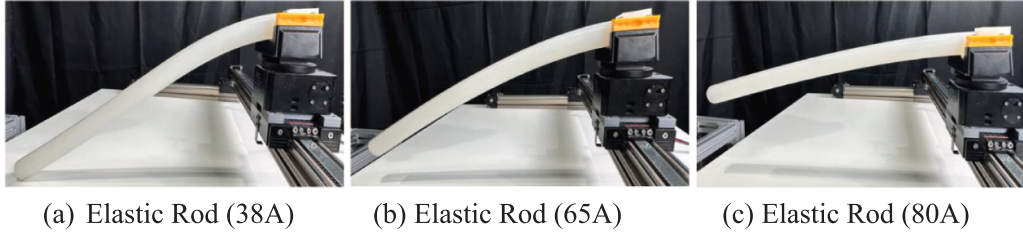


Fig. 13. Comparison of elastic rods with different stiffness levels in 1D linear motion rail-robot collaborative transportation task.

Table 6

Performance comparison of CoDoT with and without domain adapter on elastic rods with varying stiffness in the 1D rail-robot collaborative task. Oscillation Level indicates the proportion of direction reversals during robot motion. Bolded numbers represent the best performance.

Method	Normalized Object Deformation (0 ~ 1)			Average Exerted Force (N)			Oscillation Level (0 ~ 1)		
	38A	65A	80A	38A	65A	80A	38A	65A	80A
CoDoT*	0.20	0.11	0.09	2.23	1.64	1.51	0.03	0.04	0.02
w/o Domain Adapter	0.28	0.10	0.07	2.67	1.55	1.44	0.04	0.31	0.43

and trajectory jitter. In contrast, the CoDoT method, through the introduction of an adaptive admittance controller and high-frequency control based on F/T sensor data, generated continuous and smooth motion trajectories with low latency.

For Task Ease and Response Speed, Fixed-Ad showed the poorest performance. This could be attributed to its fixed admittance parameters, which result in a slow robot response to external forces and a lack of dynamic adaptation to changes in human hand movements, requiring the user to exert more force to complete the task. In contrast, CoDoT dynamically adjusts admittance parameters, significantly improving the robot's responsiveness to changes of external forces. Furthermore, its proactive motion planning model uses multi-modal information to predict the human hand's movement intent and generate corresponding robot actions, thereby reducing the operational burden on the user during task completion.

In summary, our method demonstrated exceptional performance in human-robot tasks, ensuring that the robot could quickly perceive and adapt to changes in the forces or displacements exerted by the human hand, achieving real-time interaction and dynamic adjustments. This method also enhanced the smoothness, stability, and response speed of the robot, significantly reducing the human user's operational load.

4.5.2. Generalization experiments

(1) Performance evaluation on objects with different stiffness and ablation study on domain adaptation

To evaluate the adaptability of the proposed method for handling soft rods with different stiffness, we conducted 1D Linear rail-robot collaborative transportation tests on three soft rods, each with a length of 50 cm and a diameter of 35 mm, and Shore hardness values of 38A, 65A, and 80A, as shown in Fig. 13. The elastic modulus of the three soft rods are approximately 1.2 MPa, 4.0 MPa, and 7.0 MPa, respectively. Besides, we conducted ablation experiment to validate the effectiveness of domain adapter. Each configuration was tested 30 times.

We first measured the scaling factor k (see Equation (11)) using the method described in Section 3.4 and then mapped the force/torque and tactile signals for input into the CoDoT method. In the ablation method (without domain adapter), the scaling factor k was fixed at 1, implying a constant material stiffness equivalent to the reference rod (55A).

The results in Table 6 show that the proposed method achieves relatively low deformation and exerted force across different stiffness conditions. Notably, under the 38A condition, removing the domain adapter results in significant increases in both deformation and exerted force. For 65A and 80A rods, while deformation and exerted force

slightly decreased, the oscillation level increased substantially. This increase in oscillatory behavior is likely attributed to inaccurate deformation estimation. Specifically, the same force/torque and tactile signals were interpreted as excessive deformation for the harder rods (65A and 80A) when domain adaptation was absent. As a result, the robot overcompensated during execution, often exceeding the expected motion range. This led to backward corrections in the subsequent steps, causing repeated direction reversals and thus higher oscillation levels. Conversely, for the 38A rod, insufficient motion compensation led to larger deformation and higher exerted force. These results demonstrate the generalization capability of CoDoT for handling soft objects with varying stiffness, and the critical role of domain adapter in balancing compliance and stability during transportation.

(2) Performance evaluation on objects with different material types

To further evaluate the generalization capability of the proposed approach, additional 1D linear motion human-robot collaborative transportation experiments were conducted using four types of partially deformable objects commonly encountered in industrial scenarios: aluminum alloy bar, steel coil, silicone rod and polystyrene foam board, as shown in Fig. 14. The performance comparison between our method and two baseline methods (RLDoT and Var-Ad) is summarized in Table 7. The results show that the proposed method CoDoT consistently achieves the lowest normalized object deformation and average exerted force across all object types. In contrast, RLDoT—which lacks adaptive admittance control and Var-Ad—which lacks proactive motion planning, exhibit increased object deformation and higher applied forces. These results demonstrate that the proposed method maintains adaptability across a range of material properties during human-robot collaboration.

(3) Performance evaluation on different tasks

To further evaluate the performance of the proposed method in different human-robot collaborative tasks, we conducted an obstacle-crossing transportation task and a peg-in-hole task, as shown in Fig. 15. In the obstacle-crossing task, the human and robot need to collaboratively transport the reference soft rod over an obstacle (the blue plastic cone) without any contact between the soft rod and the obstacle. The average completion time for the CoDoT method was 6.1 s, with a success rate of 100 % (30/30). In the peg-in-hole task, the human and robot cooperated to insert one end of the soft rod into the hole without any contact between the rod and the hole edge. The average completion time for this task was 7.3 s, with a success rate of 100 % (30/

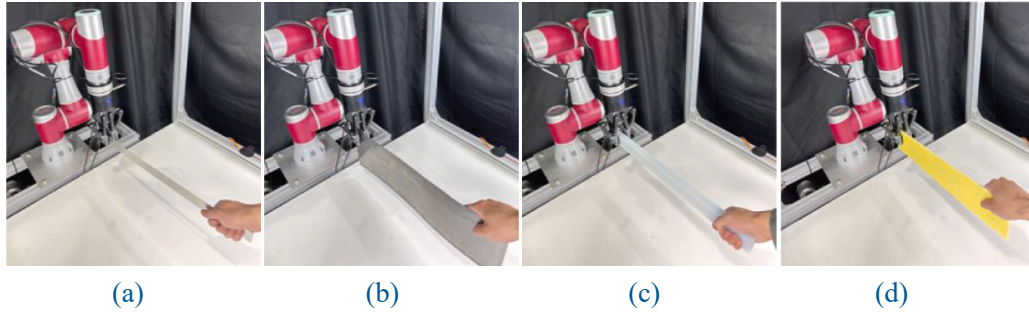


Fig. 14. Tests of four different soft objects in 1D linear motion human-robot collaborative transportation task: (a) Aluminum Alloy Bar. (b) Steel Coil. (c) Silicone Rod. (d) Polystyrene Foam Board.

Table 7

Performance of different methods in 1D linear motion human-robot collaborative transportation task with four different soft objects. Bolded numbers represent the best performance.

Method	Normalized Object Deformation (0 ~ 1)				Average Exerted Force (N)			
	Al Alloy Bar	Steel Coil	Silicone Rod	Foam Board	Al Alloy Bar	Steel Coil	Silicone Rod	Foam Board
CoDoT*	0.13	0.19	0.15	0.28	1.78	2.11	1.89	2.84
RLDoT	0.17	0.24	0.19	0.39	2.31	2.63	2.38	3.83
Var-Ad	0.20	0.27	0.24	0.45	2.64	2.89	3.15	4.40

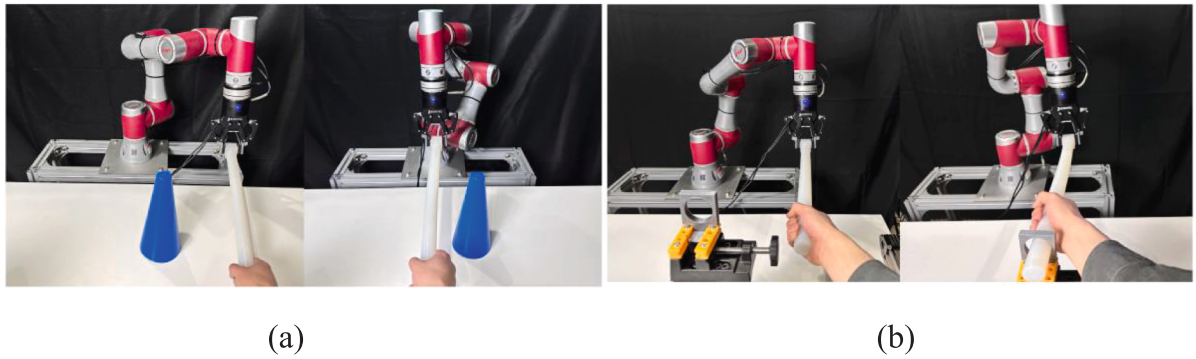


Fig. 15. Human-robot collaboration tasks: (a) Obstacle-crossing. (b) Peg-in-hole.

30).

To further assess the robustness of the proposed approach in realistic scenarios, additional tests were conducted where human operators intentionally introduced disturbances, including abrupt stops, sudden directional changes, inconsistent motions, and release of the object by the human operator. The robot consistently maintained compliant behavior without system failure or oscillatory response. The emergency detection mechanism identifies the grip release of the human operator by detecting a sharp change of z-axis force and abnormal torque derived from tactile sensor feedback. The robot achieved 100 % (30/30) success rate in disengagement detection and safe stopping, with an average response time of 0.94 s. These results demonstrate the system's ability to handle unexpected human deviations and ensure operational safety. Representative video recordings² are provided in the supplementary material to illustrate the system's adaptive performance under these conditions.

In summary, the proposed CoDoT method demonstrated excellent task completion speed and high success rates in both the obstacle-crossing tasks and peg-in-hole tasks. These results indicate the method's exceptional generalization capability and reliability in different human-robot collaboration tasks.

5. Conclusion

In this study, we propose a novel control approach (CoDoT) for human-robot collaborative transportation of deformable objects by integrating proactive robot motion planning with adaptive compliance control. Unlike vision-based methods, which may suffer from occlusions, lighting variability, and difficulty in capturing subtle deformations, our approach relies solely on robot-mounted force/torque and tactile sensors with better environmental adaptability and higher sensitivity to local deformations. By utilizing multi-modal state representations of the soft object, the robot autonomously controls its motion and achieves compliant following through an adaptive admittance controller. The proposed approach combines the adaptability and proactivity of RL-based motion planning with the collaborative stability and responsiveness of compliance control, while reducing object deformation during transportation, thereby enhancing collaboration safety. Experimental results quantitatively demonstrate the superiority of our approach across a wide range of transportation scenarios, object types, stiffness levels, and collaborative tasks. Compared to baseline methods, CoDoT achieved over 20 % reduction in normalized deformation across all tested motion patterns, and received consistently higher user evaluation scores. Besides, our method achieved 100 % success rate and average response time of 0.94 s in emergency detection tests in which the human operator released the object intentionally, confirming its high safety and

² See the video of our experiments: <https://youtu.be/W1pozEefz9E>.

robustness under human-induced disturbances. Although the experiments primarily involved objects with homogeneous material properties, our approach has potential to handle more intricate shapes and non-uniform materials. This can be achieved by integrating additional sensing modalities (e.g., vision-based systems) to capture more detailed visual information and refining object state representation to account for complex deformation patterns and material heterogeneities.

Our work enhances the compliance and operational stability of human-robot collaborative handling deformable objects in dynamic environments. It will also contribute to improved intelligence and flexibility of human-robot collaboration in the context of Industry 4.0/5.0. For example, in the medical device manufacturing field, our method could address issues related to object deformation and damage in handling delicate and flexible medical devices, ensuring that the equipment remains undamaged during transportation while minimizing harm to humans. In the logistics industry, our method could improve the accuracy and efficiency of human-robot collaborative packaging processes, ensuring the integrity of soft packaging materials and reducing the risk of damage. In electronics manufacturing, our approach offers precise control techniques for transporting delicate components, such as flexible circuit boards and soft robotic parts, addressing deformation control and stability issues during material handling.

One limitation of this work is that the current approach primarily relies on the object's intrinsic state changes and the robot's F/T and tactile feedback to support human-robot collaboration. While this approach effectively handles fundamental transportation task scenarios, it does not fully incorporate the dynamic information of human motion or environmental changes, which are critical aspects in human-robot collaborative tasks. In the future work, we plan to extend the system by integrating more modalities, such as human motion capture data and vision-based perception to further enhance the adaptability and robustness of the proposed method. This will allow the robot to better respond to human actions and environmental variations, improving its performance in more complex and dynamic human-robot collaboration scenarios.

CRedit authorship contribution statement

Qi Zhou: Writing – original draft, Conceptualization, Methodology. **Bohan Feng:** Software, Validation. **Boyan Li:** Software, Validation. **Chang Liu:** Data curation. **Yulin Chen:** Visualization. **Youyi Bi:** Project administration, Writing – review & editing, Funding acquisition.

Declaration of competing interest

The authors declare that they have no known competing financial interests or personal relationships that could have appeared to influence the work reported in this paper.

Acknowledgements

The authors would like to acknowledge the financial support from the National Natural Science Foundation of China (52575300) and the National Key R&D Program of China (2022YFB4702400).

Data availability

Data will be made available on request.

References

- [1] H. Wang, G. Wang, H. Li, J. Leng, L. Lv, V. Thomson, Y. Zhang, L. Li, L. Chen, An Automatic Unsafe States reasoning Approach towards Industry 5.0's Human-Centered Manufacturing via Digital Twin, *Adv. Eng. Inform.* 62 (2024) 102792, <https://doi.org/10.1016/j.aei.2024.102792>.
- [2] A. Zachariae, F. Plahl, Y. Tang, I. Mamaev, B. Hein, C. Wurll, Human-Robot Interactions in Autonomous Hospital transports, *Robot. Auton. Syst.* 179 (2024) 104755, <https://doi.org/10.1016/j.robot.2024.104755>.
- [3] D. Sirintuna, A. Giammarino, A. Ajoudani, An Object Deformation-Agnostic Framework for Human–Robot Collaborative Transportation, *IEEE Trans. Autom. Sci. Eng.* 21 (2) (2024) 1986–1999, <https://doi.org/10.1109/TASE.2023.3259162>.
- [4] Z. Liao, Y. Wang, Trust-based Variable Impedance Control of Human–Robot Cooperative Manipulation, *Robot. Comput.-Integr. Manuf.* 88 (2024) 102730, <https://doi.org/10.1016/j.rcim.2024.102730>.
- [5] G. Nicola, E. Villagrossi, N. Pedrocchi, Co-Manipulation of Soft-Materials estimating Deformation from Depth Images, *Robot. Comput.-Integr. Manuf.* 85 (2024) 102630, <https://doi.org/10.1016/j.rcim.2023.102630>.
- [6] D. Ge, H. Zhao, Y. Wang, D. Li, X. Li, H. Ding, Learning Compliant Dynamical System from Human demonstrations for Stable Force Control in unknown Environments, *Robot. Comput.-Integr. Manuf.* 86 (2024) 102669, <https://doi.org/10.1016/j.rcim.2023.102669>.
- [7] C. Liu, Z. Zhang, D. Tang, Q. Nie, L. Zhang, J. Song, A mixed Perception-based Human-Robot Collaborative Maintenance Approach Driven by Augmented reality and Online Deep Reinforcement Learning, *Robot. Comput.-Integr. Manuf.* 83 (2023) 102568, <https://doi.org/10.1016/j.rcim.2023.102568>.
- [8] G. Nicola, E. Villagrossi, N. Pedrocchi, In: Human-Robot Co-Manipulation of Soft Materials: Enable a Robot Manual Guidance Using a Depth Map Feedback, *IEEE, Napoli, Italy*, 2022, pp. 498–504, <https://doi.org/10.1109/RO-MAN53752.2022.9900710>.
- [9] F. Dimeas, N. Aspragathos, Online Stability in Human-Robot Cooperation with Admittance Control, *IEEE Trans. Haptics* 9 (2) (2016) 267–278, <https://doi.org/10.1109/TOH.2016.2518670>.
- [10] S. Nikoleizig, A. Vick, J. Kruger, in: Compensating Human Feedback Oscillation in Compliance Control for Industrial Robots, *IEEE, Nagoya, Japan*, 2017, pp. 221–224, <https://doi.org/10.1109/ICCART.2017.7942691>.
- [11] A.M. Khan, D. Yun, K.M. Zuhair, J. Iqbal, R.-J. Yan, F. Khan, C. Han, Estimation of Desired Motion Intention and Compliance Control for Upper Limb Assist Exoskeleton, *Int. J. Control Autom. Syst.* 15 (2) (2017) 802–814, <https://doi.org/10.1007/s12555-015-0151-7>.
- [12] Y. Hirata, Z. Wang, K. Fukaya, K. Kosuge, Transporting an Object by a Passive Mobile Robot with Servo brakes in Cooperation with a Human, *Adv. Robot.* 23 (4) (2009) 387–404, <https://doi.org/10.1163/156855309X408745>.
- [13] B. Nemeš, N. Likar, A. Gams, A. Ude, Human Robot Cooperation with Compliance Adaptation along the Motion Trajectory, *Auton. Robots* 42 (5) (2018) 1023–1035, <https://doi.org/10.1007/s10514-017-9676-3>.
- [14] R. Ikeura, H. Inooka, in: Variable Impedance Control of a Robot for Cooperation with a Human, *IEEE, Nagoya, Japan*, 1995, pp. 3097–3102, <https://doi.org/10.1109/ROBOT.1995.525725>.
- [15] Y. Zhang, K. Ding, J. Hui, J. Lv, X. Zhou, P. Zheng, Human-Object Integrated Assembly Intention Recognition for Context-Aware Human-Robot Collaborative Assembly, *Adv. Eng. Inform.* 54 (2022) 101792, <https://doi.org/10.1016/j.aei.2022.101792>.
- [16] E. Kerr, T. McGinnity, S. Coleman, “Material Recognition using Tactile Sensing,” *Expert Syst. Appl* 94 (2018) 94–111, <https://doi.org/10.1016/j.eswa.2017.10.045>.
- [17] H. Sun, T. Zhang, J. Han, H. Chu, A Fast transfer Reinforcement Learning Model for Transferring Force-based Human speed Adjustment skills to Robots for Collaborative Assembly Posture Alignment, *Adv. Eng. Inform.* 62 (2024) 102836, <https://doi.org/10.1016/j.aei.2024.102836>.
- [18] Rapetti, L., Sartore, C., Ellobaid, M., Tirupachuri, Y., Draicchio, F., Kawakami, T., Yoshiike, T., and Pucci, D., 2023, “A Control Approach for Human-Robot Ergonomic Payload Lifting,” *2023 IEEE International Conference on Robotics and Automation (ICRA)*, IEEE, London, United Kingdom, pp. 7504–7510. DOI: 10.1109/ICRA48891.2023.10161454.
- [19] H.-S. Kim, I.-M. Kim, C.-N. Cho, J.-B. Song, Safe Joint Module for Safe Robot arm based on Passive and active Compliance Method, *Mechatronics* 22 (7) (2012) 1023–1030, <https://doi.org/10.1016/j.mechatronics.2012.08.007>.
- [20] A. Bussy, P. Gergondet, A. Kheddar, F. Keith, A. Crosnier, in: Proactive Behavior of a Humanoid Robot in a Haptic Transportation Task with a Human Partner, *IEEE, Paris, France*, 2012, pp. 962–967, <https://doi.org/10.1109/ROMAN.2012.6343874>.
- [21] Aksoy, B., and Wen, J., 2024, “Collaborative Manipulation of Deformable Objects with Predictive Obstacle Avoidance.” DOI: 10.48550/arXiv.2401.16560.
- [22] D. Andronas, E. Kampourakis, K. Bakopoulou, C. Gkourmelos, P. Angelakis, S. Makris, Model-based Robot Control for Human-Robot Flexible Material Co-Manipulation, in: *2021 26th IEEE International Conference on Emerging Technologies and Factory Automation (ETFA)*, IEEE, 2021, pp. 1–8, <https://doi.org/10.1109/ETFA45728.2021.9613235>.
- [23] D. Sirintuna, A. Giammarino, A. Ajoudani, in: Human-Robot Collaborative Carrying of Objects with Unknown Deformation Characteristics, *IEEE, Kyoto, Japan*, 2022, pp. 10681–10687, <https://doi.org/10.1109/IROS47612.2022.9981948>.
- [24] S. Makris, E. Kampourakis, D. Andronas, On Deformable Object Handling: Model-based Motion Planning for Human-Robot Co-Manipulation, *CIRP Ann.* 71 (1) (2022) 29–32, <https://doi.org/10.1016/j.cirp.2022.04.048>.
- [25] A.C. Dometios, C.S. Tzafestas, Interaction Control of a Robotic Manipulator with the Surface of Deformable Object, *IEEE Trans. Robot.* 39 (2) (2023).
- [26] Narang, Y. S., Sundaralingam, B., Van Wyk, K., Mousavian, A., and Fox, D., 2021, “Interpreting and Predicting Tactile Signals for the SynTouch BioTac,” *IJRR-2022*. [Online]. Available: <http://arxiv.org/abs/2101.05452>. [Accessed: 12-Jun-2024].
- [27] P. Zhou, P. Zheng, J. Qi, C. Li, H.-Y. Lee, A. Duan, L. Lu, Z. Li, L. Hu, D. Navarro-Alarcón, Reactive Human–Robot Collaborative Manipulation of Deformable Linear

- Objects using a New Topological Latent Control Model, *Robot. Comput.-Integr. Manuf.* 88 (2024) 102727, <https://doi.org/10.1016/j.rcim.2024.102727>.
- [28] R. Laezza, Y. Karayiannidis, in: *Learning Shape Control of Elastoplastic Deformable Linear Objects*, IEEE, Xi'an, China, 2021, pp. 4438–4444, <https://doi.org/10.1109/ICRA48506.2021.9561984>.
- [29] P.M. Scheikl, E. Tagliabue, B. Gyenes, M. Wagner, Dall'Alba, D., Fiorini, P., and Mathis-Ullrich, F., Sim-to-real transfer for Visual Reinforcement Learning of Deformable Object Manipulation for Robot-Assisted Surgery, *IEEE Robot. Autom. Lett.* 8 (2) (2023) 560–567, <https://doi.org/10.1109/LRA.2022.3227873>.
- [30] J. Sanchez, C.M. Mateo, J.A. Corrales, B.-C. Bouzgarrou, Y. Mezouar, *Online Shape Estimation based on Tactile Sensing and Deformation Modeling for Robot Manipulation*, IROS-2018, IEEE, Madrid, 2018, pp. 504–511.
- [31] F. Süßerkrüb, R. Laezza, Y. Karayiannidis, in: *Feel the Tension: Manipulation of Deformable Linear Objects in Environments with Fixtures Using Force Information*, IEEE, Kyoto, Japan, 2022, pp. 11216–11222, <https://doi.org/10.1109/IROS47612.2022.9982065>.
- [32] M. Ueberle, M. Buss, Design and Control of a Hyper-Redundant Haptic Interface, in: M.H. Ang, O. Khatib (Eds.), *Experimental Robotics IX*, Springer, Berlin Heidelberg, Berlin, Heidelberg, 2006, pp. 523–532.
- [33] Q. Liu, Z. Ji, W. Xu, Z. Liu, B. Yao, Z. Zhou, Knowledge-Guided Robot Learning on Compliance Control for Robotic Assembly Task with Predictive Model, *Expert Syst. Appl.* 234 (2023) 121037, <https://doi.org/10.1016/j.eswa.2023.121037>.
- [34] J. Park, Y.-S. Shin, S. Kim, Object-Aware Impedance Control for Human–Robot Collaborative Task with Online Object Parameter Estimation, *IEEE Trans. Autom. Sci. Eng.* (2024) 1–14, <https://doi.org/10.1109/TASE.2024.3477471>.
- [35] Y. Huang, H. Chen, Z. Cui, X. Zhang, An Adaptive Impedance Control Method for Human-Robot Interaction, in: H. Yang, H. Liu, J. Zou, Z. Yin, L. Liu, G. Yang, X. Ouyang, Z. Wang (Eds.), *Intelligent Robotics and Applications*, Springer Nature Singapore, Singapore, 2023, pp. 529–539, https://doi.org/10.1007/978-981-99-6498-7_45.
- [36] L. Roveda, A. Testa, A.A. Shahid, F. Braghin, D. Piga, Q-Learning-Based Model Predictive Variable Impedance Control for Physical Human-Robot Collaboration, *Artif. Intell.* 312 (2022) 103771, <https://doi.org/10.1016/j.artint.2022.103771>.
- [37] L. Roveda, J. Maskani, P. Franceschi, A. Abdi, F. Braghin, L. Molinari Tosatti, N. Pedrocchi, Model-based Reinforcement Learning Variable Impedance Control for Human-Robot Collaboration, *J. Intell. Robot. Syst.* 100 (2) (2020) 417–433, <https://doi.org/10.1007/s10846-020-01183-3>.
- [38] X. Yu, B. Li, W. He, Y. Feng, L. Cheng, C. Silvestre, Adaptive-Constrained Impedance Control for Human–Robot Co-Transportation, *IEEE Trans. Cybern.* 52 (12) (2022) 13237–13249, <https://doi.org/10.1109/TCYB.2021.3107357>.
- [39] Q. Tang, H. Yang, W. Wang, M. Yu, L. Zhong, B. Ma, W. Yue, Grasp Compliant Control using Adaptive Admittance Control Methods for Flexible Objects, in: H. Yang, H. Liu, J. Zou, Z. Yin, L. Liu, G. Yang, X. Ouyang, Z. Wang (Eds.), *Intelligent Robotics and Applications*, Springer Nature Singapore, Singapore, 2023, pp. 515–525.
- [40] C. Sferrazza, A. Wahlsten, C. Trueeb, R. D'Andrea, Ground Truth Force distribution for Learning-based Tactile Sensing: a Finite Element Approach, *IEEE Access* 7 (2019) 173438–173449, <https://doi.org/10.1109/ACCESS.2019.2956882>.
- [41] Shi, H., Li, J., Mao, J., and Hwang, K.-S., 2023, “Lateral Transfer Learning for Multiagent Reinforcement Learning,” *TCO-2021*, 53(3), pp. 1699–1711. DOI: 10.1109/TCYB.2021.3108237.
- [42] Schulman, J., Wolski, F., Dhariwal, P., Radford, A., and Klimov, O., 2017, “Proximal Policy Optimization Algorithms.” [Online]. Available: <http://arxiv.org/abs/1707.06347>. [Accessed: 15-Apr-2024].